Many body Dynamical localization and Thermalization in Coupled kicked rotors

A Thesis
submitted to
Indian Institute of Science Education and Research Pune
in partial fulfilment of the requirements for the

BS-MS Dual Degree Programme

by

J.Bharathi Kannan

Registration No:20151077

under the supervision of

M.S Santhanam

Professor
Department of physics
IISER,Pune

Declaration

I hereby declare that the matter embodied in the report entitled Many body dynamical localisation and thermalization in coupled kicked rotor system are the results of the work carried out by me at the Department of Physics, Indian Institute of Science Education and Research, Pune, under the supervision of Dr. M S Santhanam and the same has not been submitted elsewhere for any other degree.

J.Bharathi kannan
5th year BS-MS
Department of Physics
IISER Pune

M.S Santhanam
Professor
Department of Physics
IISER Pune

Certificate

This is to certify that this dissertation entitled Many body localisation and thermalization in coupled kicked rotor system towards the partial fulfilment of the BS-MS dual degree programme at the Indian Institute of Science Education and Research, Pune represents study/work carried out by J.Bharathi kannan at Indian Institute of Science Education and Research under the supervision of Dr. M S Santhanam, Professor, Department of Physics, during the academic year 2019-2020.

J.Bharathi kannan
5th year BS-MS
Department of Physics
IISER Pune

M.S Santhanam
Professor
Department of Physics
IISER Pune

Acknowledgement

I would like to thank Dr.MS Santhanam for 2 years of great mentorship. He has been very friendly, very encouraging, made my research experience with him very wonderful. I owe a debt of gratitude to Dr.GJ Sreejith for helping me push past my limits and helped me learn a lot of new things. I thank my friends and family for putting me in a spot where I am comfortable and can focus on research. I would like to thank IISER Pune for providing me with facilities I needed like computing facility, funds to attend a few international conferences. I would like to acknowledge the INSPIRE Scholarship from DST.

Abstract

Due to the absence of conservation of energy in periodically driven systems with interactions they are expected to heat up indefinitely. We have shown that this is not generally the case with the help of three types of interactions in the kicked rotor model. We can achieve a transition between dynamical localisation and delocalisation by varying some parameters in the system. These systems show similar dynamics in momentum space on comparing it with impurity models in position space, this can be explained via a map between coupled kicked rotors and impurity lattice model in momentum space.

Contents

List of Figures

1 Introduction

Periodically driven systems are all around us and within us. For example, our ability to perceive sound is due to a periodic perturbation of the sound wave, through which energy is transferred to our body and activates a chain of processes which result is our ability to hear. Our body is a very big self-periodically driven system, as the periodic contractions of our heart, controls our metabolism. Most of the classically driven systems have an effect of heating, kinetic effects, but in the quantum regime, we observe non-trivial effects which don't have a classical counterpart [1].

Periodically driven systems are studied with the help of Floquet engineering [2], with the help of recent theoretical and experimental efforts has lead to the observation of new quantum phases of matter. A few examples are quantum wire made of cold atoms [3], superconductivity in cuprates [4], superfluidity [5] and floquet insulators [6]. The periodically driven system which we are interested in is of a delta-kicked quantum rotor, which is one of the well-known floquet systems in quantum chaos. The system is tunable by a main free parameter known as the kick strength (K). For sufficiently large kick strengths this system shows dynamical localisation in momentum space in the quantum regime but shows diffusive behaviour in the corresponding counterpart in the classical regime. This behaviour makes it a very interesting system to study as dynamical localisation arises due to the pure quantum nature of the system, might help us understand the fundamentals of quantum mechanics itself. There are also other tunable parameters in the system like effective planks constant of the system ($\hbar$) and time period of kicking (T). We can obtain very interesting behaviour like quantum resonance and quantum anti-resonance in momentum space with the help of these parameters.

In this work, we have carried out a study on the dynamics of kicked rotors in the presence of interaction in configuration space, temporal space and momentum space separately. The main question we are interested to answer is "whether in the presence of interactions dynamical localisation is preserved or lost to a thermal phase". In general, due to the absence of energy conservation in the presence of interactions, periodically driven systems are expected to heat up in time to a thermal state[7]. But this is always not the case, for example in weakly driven many-body systems [8] and when the driving frequency is very high the relaxation time scale is much larger than the driving time scale.

The motivation to this work is from the mapping introduced by Fishman et, al [9], which maps the dynamics of a time-dependent quantum kicked rotor to a time-independent 1d lattice model in momentum space with quasi-random onsite potentials and short-ranged hopping terms, similar to an Anderson impurity model in 1d[9]. This mapping can be extended to kicked rotors with interactions in configuration space[10], Temporal space[11] and momentum space[12]. This mapping gives us a rough idea on what dynamics should be expected by comparing it with the existing impurity lattice models in position space like the Anderson model, Aubry-Andre model, Lloyd model.

In this work, we have studied the dynamics coupled kicked rotors model by studying the floquet dynamics and also by analysing the spectral properties of the mapped lattice model in momentum space.

We have observed the absence of thermalization even in the presence of interaction and there is also a transition between energy saturation and unbound energy growth in all the three types of couplings.

The chapters of the thesis are organized as follows.

- In Chapter 1: A general introduction to classical and quantum chaos, along with Floquet formalism and introduction to the Anderson impurity model is given.
- In Chapter 2: Dynamics of the kicked rotors model is explained in its classical and quantum regime. The mapping of quantum kicked rotor to an Anderson type tight-binding model in 1d is explained.
- In Chapter 3: The classical and quantum dynamics of two spatially coupled kicked rotors is discussed. The corresponding map to a two dimensional Anderson type tight-binding model is discussed along with the study of its spectral statistics.
- In Chapter 4: The classical and quantum dynamics of three spatially coupled kicked rotors is discussed. The mapping to a three dimensional Anderson type tight-binding model is discussed along with the study of spectral statistics in this model.
- In chapter 5: Quantum resonance in Quantum kicked rotor (primary resonance, secondary resonance and anti-resonance) is discussed.
- In chapter 6: Quantum resonance in spatially coupled kicked rotors is studied.
- In chapter 7: Dynamics of Temporally coupled or Quasi-periodic kicked rotor is discussed, along with mapping of the quasi-periodic kicked rotor with three incommensurate frequencies to a three-dimensional impurity model is explained.
- In chapter 8: Kicked rotors coupled in momentum space is studied and its mapping to an interacting Aubry-Andre type model is discussed.
- In the Conclusions, we summarize the results presented in the thesis and discuss possible directions which are left for future work.

1.1 Classical Chaos

There are many systems in classical physics whose dynamics is called chaotic, for example, the double pendulum [13], the Sinai's billiard [14]. These systems are non-integrable systems and chaotic behaviour arises due to the nonlinear form of interactions between more than two components of the system. These chaotic systems are very sensitive to the initial conditions of evolution. In regular systems, smaller uncertainties in the initial condition don't really affect the final state of the systems, but in chaotic systems, they get affected profoundly. In this sense, the evolution of a chaotic system is often considered unpredictable, due to our inability to determine the initial state with infinite precision. This behaviour can be seen with the help of classical billiards in figure 1.1 [15].

In classical chaotic systems, trajectories in phase space which are close to each other initially start to diverge under time and the rate of divergence is determined by the parameters known as Lyapunov exponent[16].

Let two trajectories in phase space with initial separation vector $\delta\mathbf{X}_0$ diverge at a rate given by

$$|\delta\mathbf{X}(t)| \approx e^{\lambda t} |\delta\mathbf{X}_0| \tag{1.1.1}$$

The rate of separation of trajectories can be different for different orientations of the initial separation vector. Thus, there is a spectrum of Lyapunov exponents, equal in number to the dimensionality of the phase space. The dynamics of the system is determined by Maximal Lyapunov exponent (MLE) which is the largest one. If the MLE is positive then the dynamics is chaotic. If we consider an arbitrary initial state separation vector and look at its components will typically contain some component in the direction associated with the MLE, and because of the exponential growth rate, the effect of the other exponents will be diminished at a long time.

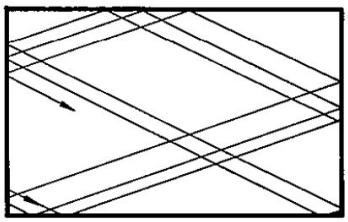

(a) Rectangular Billiard(Regular Trajectory)

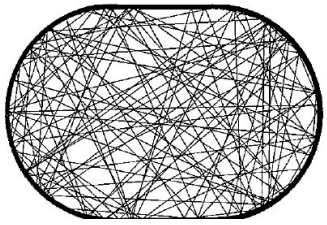

(b) Sinai Billiard(Chaotic Trajectory)

Figure 1.1: Trajectory of particles in billiards

1.2 Quantum Chaos

Quantum chaos is the study of the dynamics of quantum systems whose classical counterparts are chaotic. This name is misleading from distance, the paradox in this name is the source of interest it has provoked. If we're studying the long time behaviour of a classically chaotic system its small details get amplified but this is completely different to what happens in the quantum regime. Quantum interference's tend to, suppress classical chaos and this is what creates the paradox in the name itself. This property of the system has made it a suitable example to examine the fundamentals of quantum mechanics. Because what quantum chaos means is directly related to the difference between classical and quantum dynamics of a system. It's in particular related to the question of how the classical dynamics of a system emerge from the reality of quantum mechanics.

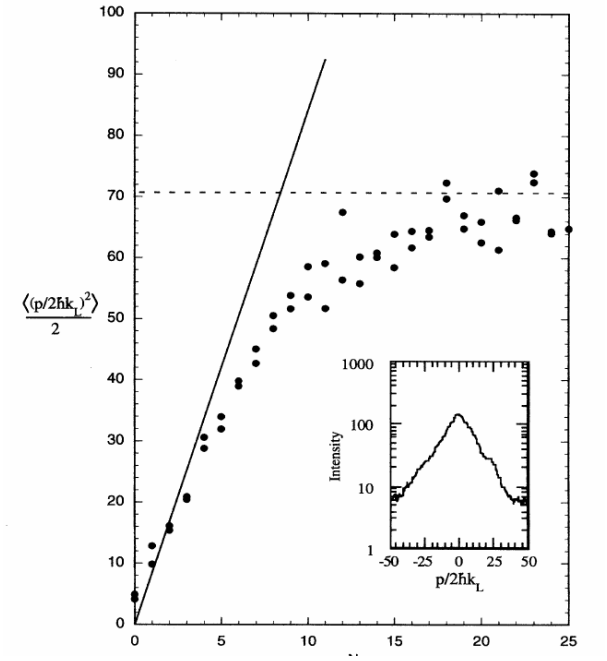

Figure 1.2: Dynamical localisation in kicked rotor
[17]

In the studies of the kicked rotor, it was discovered that the quantization of classically chaotic systems can lead to the suppression of chaos. This is one of the most spectacular results in quantum chaos research. The classical dynamics of the kicked rotor is described by the famous standard map, and it has been known for some time that for sufficiently large kick strengths of the classical system show diffusive behaviour. But for its quantum mechanical counterpart the diffusion is stopped after some time by a process called dynamical localisation as shown in figure 1.2. Dynamical localisation of electrons [18] and atoms[19] has also been experimentally realised.

The kicked rotor system belongs to floquet systems, Fishman et,al[9] found a relation between kicked rotor systems and Anderson model, this mapping implies that dynamical localisation is a special case of Anderson localisation.

Time-periodic systems have discrete time-translation invariance and their dynamics are constrained by conservation laws. The energy of time-dependent Hamiltonian systems are not conserved but the dynamics of such systems are governed by the hermitian operator know as the floquet operator, its eigenvalues the quasi-energies are conserved quantities [20].

1.3 Floquet Theory

For Hamiltonian's periodic in time ,

$$H(t) = H_0 + V(t) \tag{1.3.1}$$

where $V(t)$ is the time dependent potential with period T i,e.. $V(t+T) = V(t)$.

Using Floquet theory it is possible to describe the time evolution of quantum systems in terms of a Floquet map that connects the state $\phi(t)$ at time t to the state $\phi(t+T)$ at time $t+T$. The main advantage for kicked rotor systems is that this floquet map can be constructed analytically, in most other cases it has to be constructed numerically.

As Hamiltonian is periodic with time T, now we can use separation of variables to solve the corresponding time-dependent Schrödinger equation.

$$i\hbar\frac{\partial\phi}{\partial t} = H(t)\phi \tag{1.3.2}$$

Let discrete-time translation operator be A_T .

$$[H, A_T] = 0 \tag{1.3.3}$$

Now we can find solutions ϕ_n which are simultaneous eigenfunctions of Hamiltonian and Discrete-time translation operator A_T.

$$A_T\phi_n(x,t) = \phi_n(x,t+T) \tag{1.3.4}$$

$$\phi_n(x,t+T) = \beta_n\phi_n(x,t) \tag{1.3.5}$$

β_n are pure phase factors for stationary solutions.

$$\phi_n(x,t+T) = e^{-i\alpha_n}\phi_n(x,t) \tag{1.3.6}$$

$$\phi_n(x,t) = e^{\frac{-i\omega_n t}{\hbar}}\chi_n(x,t) \tag{1.3.7}$$

where $\chi_n(x,t) = \chi_n(x,t+T)$ and $\omega_n = \frac{\alpha_n \hbar}{T}$, this is called floquet theorem, similar to Bloch's theorem in periodic lattices.

α_n are called the floquet phases which are defined only up to integer multiples of 2π, therefore the quasi-energies ω_n are defined only up to integer multiples of $\frac{2\pi\hbar}{T}$.

The time evolution operator $U(t)$ is defined as

$$\phi(x,t) = U(t)\phi(x,0) \tag{1.3.8}$$

where $\phi(x,t)$ is a solution of the Schrodinger's equation (1.3.2)

$$i\hbar\dot{U} = HU \tag{1.3.9}$$

U is unitary for hermitian Hamiltonian, it can be shown that as the Hamiltonian has discrete-time invariance.

$$U(nT) = [U(T)]^n \tag{1.3.10}$$

As $U(T)$ is unitary and it can be diagonalized with a unitary transformation, which yields the floquet phases (α_n) [1]

$$(U_D)_{nn} = e^{-\imath\alpha_n} \tag{1.3.11}$$

These eigenphases of U turns out to be the floquet phases. So we just need to diagonalise the unitary evolution operator to determine the dynamics of floquet systems.

1.4 Anderson Tight Binding Model

Anderson tight-binding model is a lattice model with nearest neighbour hopping and onsite potentials randomly chosen from a uniform distribution. Here we review the properties Anderson impurity model because the quantum kicked rotor model can be mapped to a tight-binding model in 1d with quasi-random onsite impurities in momentum space (similar to Anderson model in position basis)[9] and this mapping has been studied in detail.

Hamiltonian of the Anderson model in 1d is given by [21]:

$$H = \sum_{n=0}^{L} w_n|n\rangle\langle n| + t(|n\rangle\langle n+1| + |n+1\rangle\langle n|) \tag{1.4.1}$$

Where w_n is the onsite potential which is randomly drawn from a distribution of $[-W,W]$, W is called the disorder strength, t is the nearest neighbour hopping strength, in our calculation its taken to be 1 and L is the size of the lattice in 1d. Similarly, 2d and 3d Anderson models can be constructed.

All the eigenstates in 1d Anderson model are localised for even very small values of disorder strength (W). Similarly, localisation is observed in 2d Anderson model but in two limits Weak localisation (for

small values of W) and Strong localisation (for large values of W). Something peculiar happens in case of 3d lattice, there is a transition from delocalised states (Weak disorder strength) to localised states (Large disorder strength) this is called as a Metal-Insulator transition.

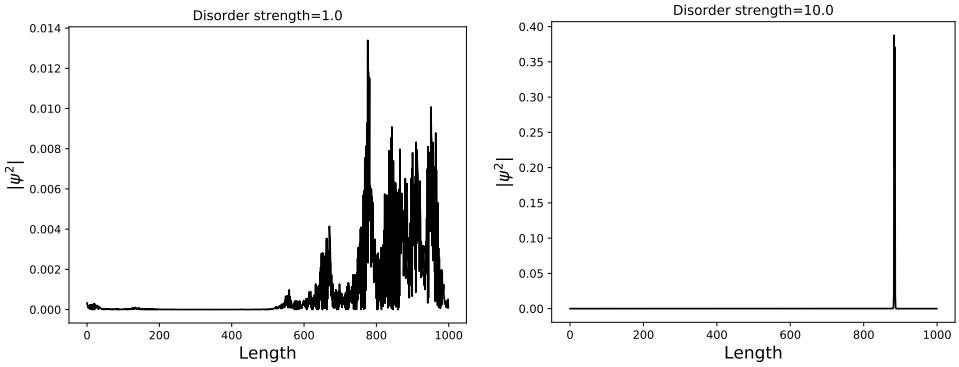

(a) L=1000, W=1 (b) L=1000, W=10

Figure 1.3: Eigenstates in 1d Anderson Model

In the above figure 1.3 $|\psi^2(x)|$ is plotted for a randomly picked eigenstate $\psi(x)$ in 1d Anderson model. (a) Eigenstates are localised even for small value disorder strength $(W = 1)$ and (b) Strongly Localised for high disorder strength $(W = 10)$.

1.5 Spectral Statistics

Its a study on the statistical quantities which can be obtained from the eigenvalues and eigenvectors of the Hamiltonian of interest. These quantities give information about the general dynamics of the system like whether it is localised or delocalised.

Inverse Participation Ratio

Inverse participation ratio is one of the quantities which can be computed when the eigenstates of the system are known. Its basically the 2nd order moment of the distribution $|\psi(x)|^2$, where $\psi(x)$ is an eigenstate of the system.

Inverse Participation Ratio (IPR) defined for each eigenstate is given by:

$$IPR = \sum_x |\psi(x)|^4 \tag{1.5.1}$$

where $\psi(x)$ is the eigenstate of the Hamiltonian in the position basis. Later in case of Kicked rotor, we will be considering eigenstates in momentum basis, the same definition of IPR holds there as well.

In these below calculations of the Anderson model, we will deal with Inverse IPR rather than IPR to clearly show the scaling with systems linear size (L).

d-Dimensional Anderson model

If all the eigenstates are completely delocalised, then any eigenstate $|\psi(x)|^2 = \frac{1}{L^d}$ for a system of linear size (L).

The Inverse IPR for a particular eigenstate $\psi(x)$ is given by:

$$\frac{1}{\sum_x |\psi(x)|^4} \tag{1.5.2}$$

Instead of randomly picking up a eigenstate and calculating IPR we are going to average the Inverse IPR over all the eigenstates to reduce the significance of any extreme cases.

For completely delocalised eigenstates, the Average of Inverse of IPR is given by:

$$\frac{1}{L^d} \sum_{\psi} [\frac{1}{\sum_x |\psi(x)|^4}] = L^d \tag{1.5.3}$$

For perfectly localized states $\psi(x) = \delta_{x,x_0}$, the Average Inverse IPR yields

$$\frac{1}{L^d} \sum_{\psi} [\frac{1}{\sum_x |\psi(x)|^4}] = 1 \tag{1.5.4}$$

For a exponentially localized states $\psi(x) = \exp(\frac{-x}{\chi})$ with localisation length χ, Average of Inverse IPR behaves as

$$\frac{1}{L^d} \sum_{\psi} [\frac{1}{\sum_x |\psi(x)|^4}] \approx \chi^d \tag{1.5.5}$$

1d Anderson model

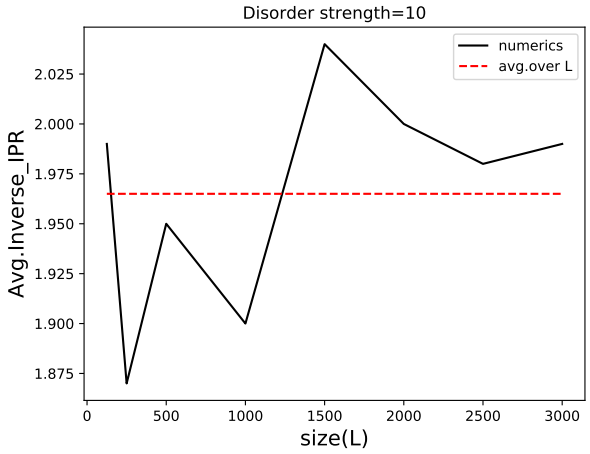

Figure 1.4: Average Inverse IPR vs System size (1d)

The above figure 1.4 shows how Average Inverse IPR depends on the system size, and we can conclude that the eigenstates are localized as there is no scaling with system size seen. From equation (1.5.5) we can say the localisation length ≈ 2 if the eigenstates are exponentially localised.

2d Anderson model

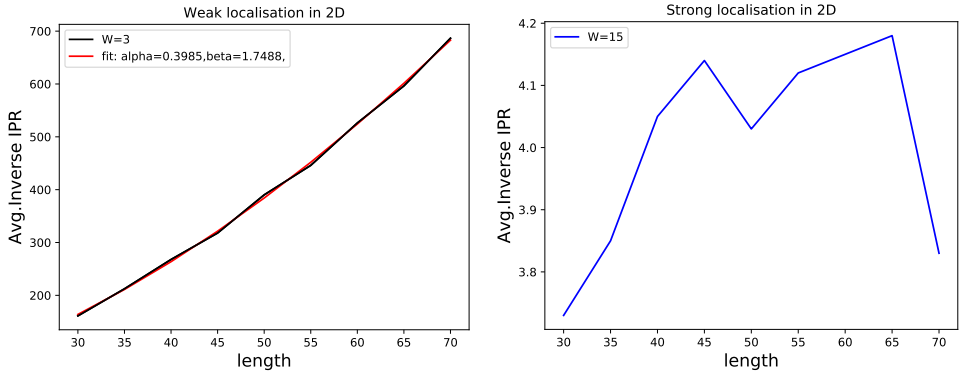

(a) Weak localisation W = 3 (b) Strong localisation W = 15

Figure 1.5: Average Inverse IPR vs System Size (2d)

In the above figure Average Inverse IPR is plotted versus systems size for a 2d Anderson model is weak (a) and strong (b) disorder limits.

From the figure 1.5 (a) we can conclude that in weak localised limit of 2d Anderson model the dynamics is diffusive (Fit in the plot is a power-law fit with parameters α and β : Avg.Inverse.IPR $=\alpha\, L^{\beta}$,scaling parameter $\beta \approx 1.75$). In case of strong localisation limit in 2d Anderson model from figure 1.5 (b), Average Inverse IPR doesn't scale with system size implying the localised nature of eigenstates.

3d Anderson model

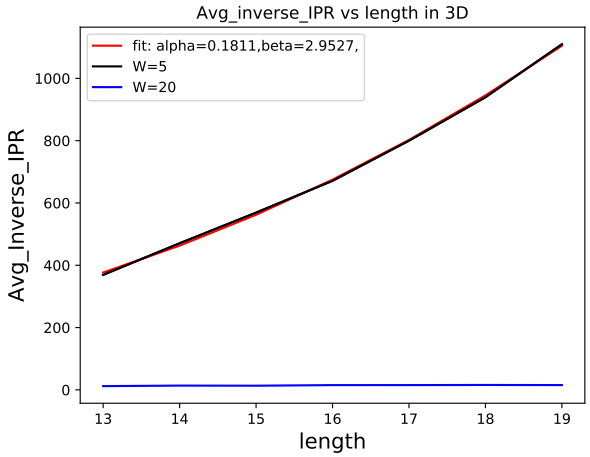

Figure 1.6: Average Inverse IPR vs System Size (3d)

In the above figure 1.6 the Average Inverse IPR is plotted versus system linear size (L) for disorder strengths $W = 5$ and $W = 20$. The average inverse IPR has a power law fit for the weak disorder case ($W = 5$), Average Inverse IPR = $\alpha\ L^{\beta}$. We can see the scaling of average inverse IPR with system size (L) goes as $\beta \approx 3$ in the metallic regime (weak disorder W=5) and doesn't show any scaling in the insulator regime (Strong disorder W = 20). This is the metal-insulator transition in 3d Anderson model.

Average Level spacing ratio

The Average level spacing ratio is effective way to determine whether the dynamics is localised or ergodic if all the eigenvalues of the system are known. The Average Level spacing ratio is defined as :

$$\langle r \rangle = \frac{1}{L^d - 2} \sum_{\alpha=1}^{L^d-2} \frac{\min\{\gamma_\alpha, \gamma_{\alpha+1}\}}{\max\{\gamma_\alpha, \gamma_{\alpha+1}\}} \tag{1.5.6}$$

where, $\gamma_\alpha = \omega_{\alpha+1} - \omega_\alpha$, ω_α are the eigenvalues written in increasing order, L is the linear size of the system and d is the dimension of the lattice.

The value of Average level spacing ratio ($< r >$) can be calculated with the help of probability distribution of level spacing ratios $P(r)$[22].

$P(r)$ for Gaussian orthogonal ensemble (Ergodic system)

$$P(r) = C\frac{(r + r^2)}{(1 + r + r^2)^{5/2}} \tag{1.5.7}$$

and the average level spacing ratio calculated from this distribution is $< r > \approx 0.530$.

$P(r)$ for integrable system is given by :

$$P(r) = \frac{1}{(1+r)^2} \tag{1.5.8}$$

and the average level spacing ratio calculated from this distribution is $< r > \approx 0.386$.

Average Level spacing ratios for Anderson impurity model

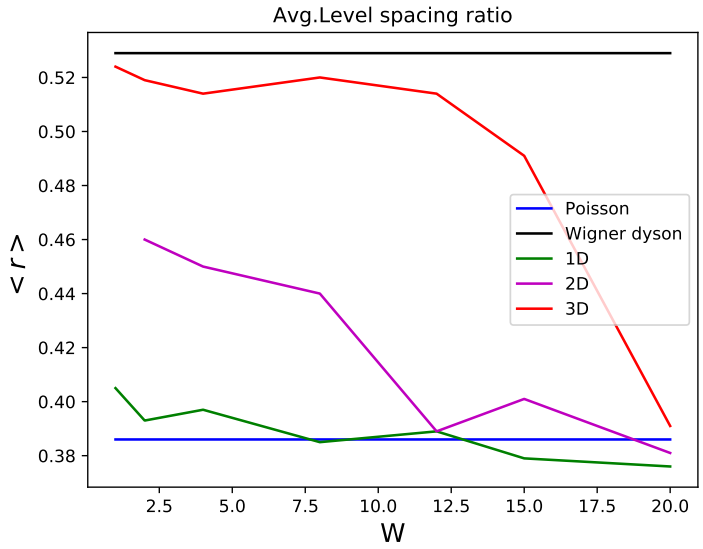

Figure 1.7: Average Level spacing ratio vs Disorder strength (W)

In the above figure 1.7 average level spacing ratio is plotted vs disorder strength (W) for 1d, 2d and 3d Anderson models, the following results can be inferred from the plot :

In 1d Anderson model $< r > \approx 0.386$ for almost all values of disorder this, the corresponding level spacing distribution will be Poisson. This explains the localised behaviour for all strengths of disorder in 1d.

In 2d Anderson model for lower value of disorder strength the dynamics is weakly localised ($< r > \approx$ 0.44) and for higher value of W it attains strong localisation ($< r > \approx 0.386$) .

In 3d Anderson model, there is a metal to insulator transition around $W = W_c \approx 16$ of the disorder strength. The corresponding transition in terms of level spacing distribution is Wigner-Dyson to Poisson.

2 Kicked Rotor Model

The kicked rotor is a very well studied model in classical and quantum chaos studies as the dynamics of this system can be easily obtained even analytically in some cases. It's a particle that is constrained to move on a ring and besides, there is a delta-kicking introduced on the particle periodically.

The Hamiltonian of the system is:

$$H(t) = \frac{L^2}{2I} + K\cos\theta \sum_n \delta(t - nT)$$

where L is the angular momentum, θ is the angular variable, I is the momenta of inertia, K is the kick strength and T is the kicking period.

2.1 Classical kicked rotor

The kicked rotor belongs to the Hamiltonian systems. The equations of motion are obtained from the canonical equations

$$\dot{\theta} = \frac{\partial H}{\partial L} \quad \dot{L} = -\frac{\partial H}{\partial \theta} \tag{2.1.1}$$

$$\dot{\theta} = L, \quad \dot{L} = K\sin\theta \sum_n \delta(t - n) \tag{2.1.2}$$

Here I and T have been normalized to one.

As L changes discontinuously, the equations of motion define a map for the dynamical variables θ, L.

This is chirikov's map

$$\theta_{n+1} = \theta_n + L_{n+1} \tag{2.1.3}$$

$$L_{n+1} = L_n + K\sin\theta_n \tag{2.1.4}$$

Using the chirikov's map we have obtained the phase space in angular momentum (L) and angle variable (θ). We can also obtain the average energy of the classical kicked rotor $< E(n) >= \frac{<L^2(n)>}{2}$ after n kicks. The averaging is done over number of initial conditions.

Classical phase space plots

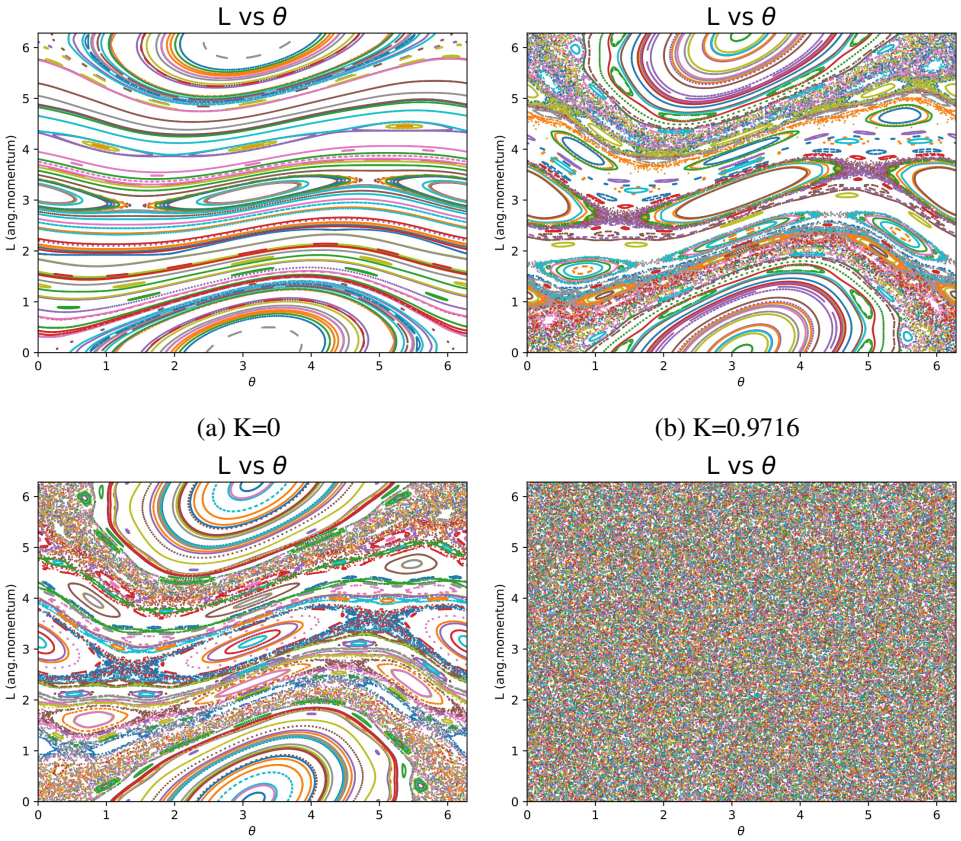

(a) K=0

(b) K=0.9716

(c) K=1

(d) K=8

Figure 2.1: Phase space plots of kicked rotor.

In the above figure 2.1 the phase space of kicked rotor is plotted using the iteration map between L and θ from equations (2.1.3) and (2.1.4) for varying kick strength (K).

For small values of K the classical dynamics of the rotor is regular, for most of the initial values of θ and L. The motion in phase space proceeds on the so-called invariant tori, where L varies only a little, while θ takes all values between 0 and 2π with about equal probability. On increasing kicking strength (K) more and more tori breaks up, until above a critical value of $K = K_c = 0.9716$ .. the last invariant torus will have been destroyed.

There are, however, still regular regions in the phase space. For $K \geq 5$ finally, the major part of the phase space has become chaotic.

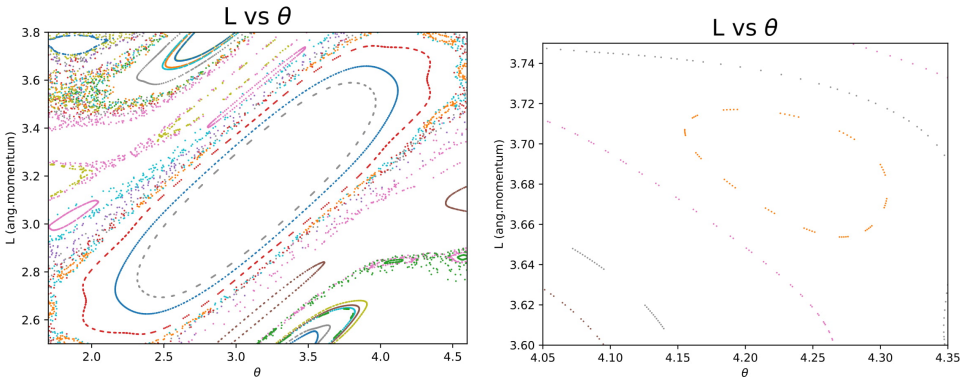

(a) K=1, Secondary Island (b) K=1, Tertiary Island

Figure 2.2: Islands in Kicked rotor

In the above figure 2.2 a secondary island (a) and a tertiary island (b) are shown from the phase space of kicked rotor.

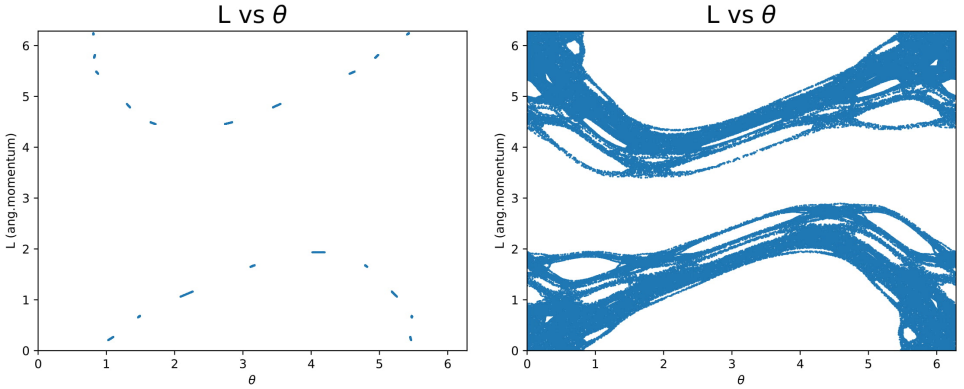

(a) K=1, Regular trajectory (b) K=1, Chaotic trajectory

Figure 2.3: Trajectories in Kicked rotor

For lower values of kicking (K =1) some parts of the KAM tori is destroyed but there are also some regular regions. From the above figure 2.3 at K =1, (a) shows a regular trajectory and (b) is a chaotic trajectory.

Momentum distribution of classical kicked rotor

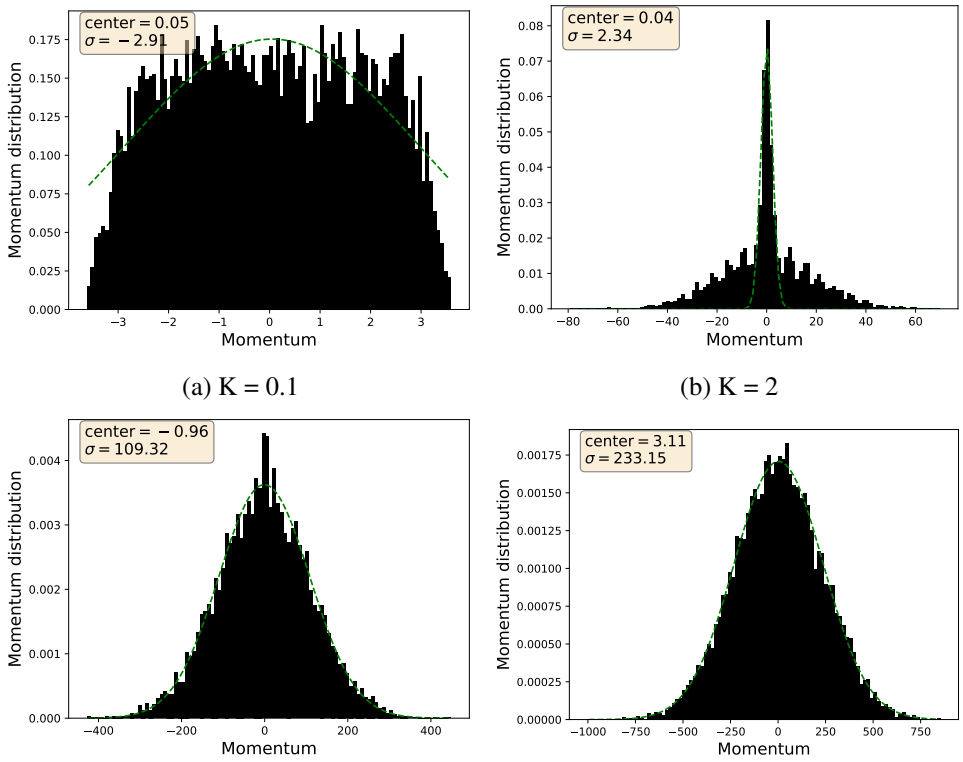

(a) K = 0.1

(b) K = 2

(c) K = 5

(d) K = 8

Figure 2.4: Momentum distribution of classical kicked rotor

In figure 2.4 the distribution of classical momenta in different momentum values after 1000 kicks is plotted for different values of kick strength along with a Gaussian fit, as the Gaussian distribution of momentum is a indication of dynamics being diffusive in momentum space.

Gaussian distribution:

$$f(m) = A \exp\left(-\frac{(m-\mu)^2}{2\sigma^2}\right)$$

where m is the momentum space, μ is the centre of Gaussian distribution and σ is the standard deviation of Gaussian distribution.

The momentum at a long time is bound by the regular structures of KAM tori for small values of kicking ($K \leq 1$). On increasing the kick strength (K) the spread in the classical momentum of the system increases.

The central peak is present in the momentum distribution for kick strengths ($1.5 \leq K \leq 5$), due to the presence of stable islands in the phase space. The central peak also disappears slowly and for $K = 8$ the momentum distribution is almost a perfect Gaussian, a characteristic feature of chaotic diffusion.

$< L^2 >$ vs time for classical kicked rotor

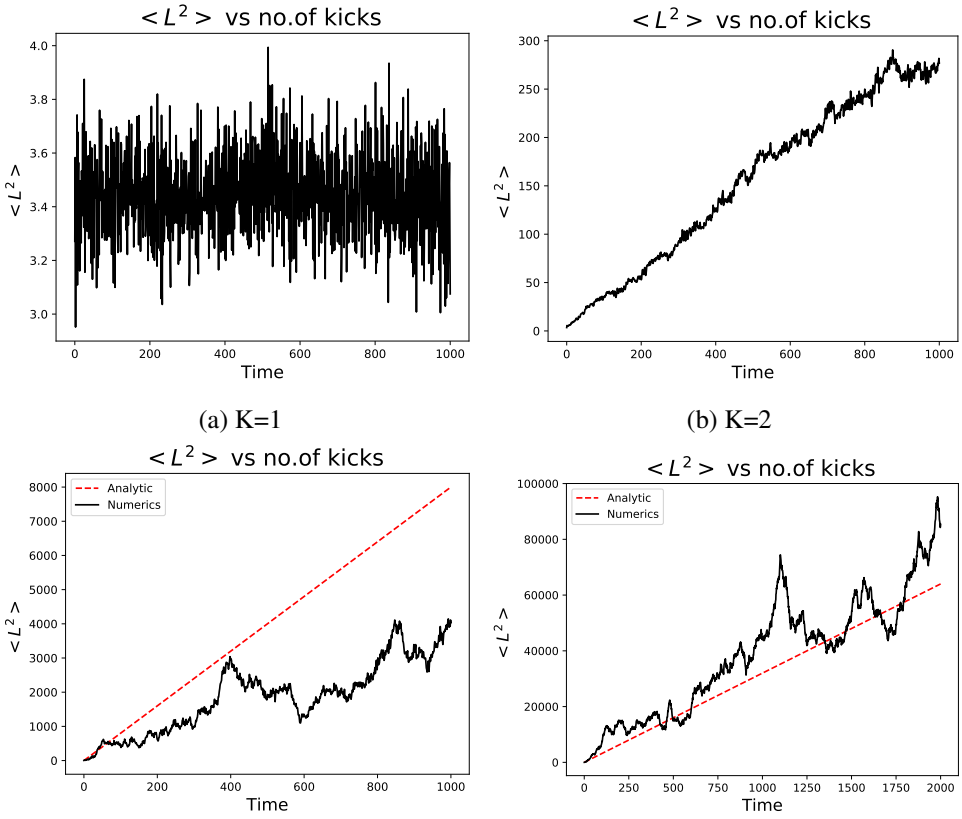

(a) K=1 (b) K=2

(c) K=4 (d) K=8

Figure 2.5: $< L^2 >$ vs time for Classical kicked rotor.

In the above figure 2.5 the average of angular momentum square $< L^2 >$ is plotted versus time (no.of kicks). Here average is done over 10 initial conditions.

For low values of kick strength, we observe classical trapping due to the presence of stable KAM tori. On increasing the kick strength the KAM tori breaks leading to a diffusive behaviour of $< L^2 >$.

Diffusion Constant for classical kicked rotor

The diffusion constant can be calculated as follows:

$$D = \frac{1}{2\pi}\int_0^{2\pi} (L_{n+1} - L_n)^2 \, d\theta_n \tag{2.1.5}$$

from equation (2.1.4)

$$D = \frac{1}{2\pi}\int_0^{2\pi} (K \sin\theta_n)^2 \, d\theta_n = \frac{K^2}{2} \tag{2.1.6}$$

In this calculation, we have assumed a uniform distribution for θ but this is not true, so there are also higher-order terms in the diffusion constant expression.

$$D = \frac{K^2}{2}\left[1 - 2\mathscr{J}_2(K) + 2\mathscr{J}_2(K)^2\right] \tag{2.1.7}$$

where $\mathscr{J}_2$ is the second order Bessel function of first kind.

For higher values of kicking ($K = 8$), the phase space is completely chaotic hence the approximation used in the calculation of first-order diffusion constant in equation(2.1.6) holds good as the analytic data fits the numerics well as seen from figure 2.5 (d). But for lower values of kicking ($K = 4$), the first-order approximation doesn't hold good due to the presence of some regular regions as seen from the figure 2.5 (c).

2.2 Quantum kicked rotor

We now study the quantum version of the same time-dependent system of periodically kicked rotors. The general form of the Hamiltonian of a N kicked rotors with or without coupling is given by:

$$H = T_0(\{\hat{L}_i\}) + V(\{\hat{\theta}_i\}) \sum_{n=-\infty}^{+\infty} \delta(t - nT) \tag{2.2.1}$$

$\{\hat{\theta}_i\} = (\hat{\theta}_1, \hat{\theta}_2, ..., \hat{\theta}_N)$ and $\{\hat{L}_i\} = (\hat{L}_1, \hat{L}_2, ..., \hat{L}_N)$ are the operators corresponding to angle and angular momenta of the rotors.

$\hat{L}_i \equiv -\imath\hbar\partial/\partial\theta_i$, $T_0\left(\{\hat{L}_i\}\right) = \sum_i \hat{L}_i^2/2I_i$ is the general form of the kinetic energy.

$V(\theta_i)$ is a periodic potential function, T is the kicking period.

In all our calculation we have taken $T = 1$ and $I = 1$. The Schrodinger equation of wave function in angle representation is

$$i\hbar\frac{\partial}{\partial t}\phi\left(\{\theta_i\}, t\right) = \left(T_0\left(\{\hat{L}_i\}\right) + V\left(\{\theta_i\}\right) \sum_{n=-\infty}^{+\infty} \delta(t - n)\right) \phi\left(\{\theta_i\}, t\right) \tag{2.2.2}$$

Single Quantum kicked rotor

$V\left(\{\theta_i\}\right) = V(\theta_1)$, Unlike the classical case the quantum system needs two dimensionless parameters to specify its motion. We take them to be

$$\alpha := \frac{\hbar T}{I} \qquad \beta := \frac{K}{\hbar} \tag{2.2.3}$$

As mentioned above $T = 1$ and $I = 1$ so,

$$\alpha := \hbar \quad \beta := \frac{K}{\hbar} \tag{2.2.4}$$

The time-dependent Schrodinger equation in these units will be

$$\imath \frac{\partial}{\partial t}\phi(\theta,t) = \left(-\frac{\alpha}{2}\frac{\partial^2}{\partial \theta^2} + \beta V(\theta) \sum_{n=-\infty}^{+\infty} \delta(t-n) \right) \phi(\theta,t) \tag{2.2.5}$$

let the wave function in momentum basis be

$$\phi_m := \langle m|\phi\rangle$$

where $|m\rangle = (\sqrt{2\pi})^{-1} e^{im\theta}$, is eigenstate of angular momentum operator ($\hat{L}$),

$$\hat{L}|m\rangle = m\hbar|m\rangle$$

The system is effectively a free rotor between kicks, and thus the time evolution of wave function in momentum basis is trivial. We denote the wave function just before the t^{th} kick as $\phi^-(t)$ and just after the t^{th} kick as $\phi^+(t)$. Between the kicks, the motion is free evolution with kinetic energy

$$\phi_m^-(t+1) = e^{\frac{-iT_0(m)}{\hbar}} \phi_m^+(t) \tag{2.2.6}$$

During the kick we consider strong kicks such that the kinetic energy is infinitesimal and can be ignored, which leads to trivial evolution of wave function in position basis

$$\phi^+(\theta,t) = e^{\frac{-iV(\theta)}{\hbar}} \phi^-(\theta,t) \tag{2.2.7}$$

We can obtain wave function in momentum basis from wave function position basis or vice-versa through Fourier transforms.

$$\phi_m(t) = \frac{1}{\sqrt{2\pi}} \int_0^{2\pi} d\theta e^{-im\theta} \phi(\theta,t) \tag{2.2.8}$$

$$\phi(\theta,t) = \sum_m e^{im\theta} \phi_m(t) \tag{2.2.9}$$

Combing the above equations(2.2.6) and (2.2.7) gives us

$$\phi_n^+(t+1) = \sum_{m=-\infty}^{\infty} J_{n-m} \exp\left(-i\hbar m^2/2\right) \phi_m^+(t) \tag{2.2.10}$$

where

$$J_{n-m} = (2\pi)^{-1} \int_0^{2\pi} d\theta e^{-i(m-n)\theta} e^{\frac{-iV(\theta)}{\hbar}} \tag{2.2.11}$$

So far in all the above steps we haven't specified the functional form of $V(\theta)$. For a kicked rotor system the potential of the form $V(\theta) = K\cos(\theta)$.

$$J_{n-m}(\beta) = (2\pi)^{-1} \int_0^{2\pi} d\theta e^{-i(m-n)\theta} e^{-i\beta\cos\theta} \tag{2.2.12}$$

The above mentioned integral $J_{n-m}(\beta)$ in equation (2.2.12) can be related to the well known Bessel function of the first kind ($\mathscr{J}_{n-m}(\beta)$) .

$$J_{n-m}(\beta) = (2\pi)^{-1} \int_0^{2\pi} d\theta e^{-i(m-n)\theta} e^{\frac{-iK\cos\theta}{\hbar}} = \imath^{n-m} \mathscr{J}_{n-m}(\beta) \tag{2.2.13}$$

The floquet evolution operator from equation (2.2.10) is given by

$$F_{mn} = \exp(-\imath\hbar m^2/2)\imath^{n-m} \mathscr{J}_{n-m}(\beta) \tag{2.2.14}$$

The evolution operator in equation (2.2.14) becomes effectively a banded matrix as the matrix element $\mathscr{J}_{n-m}(\beta) \to 0$ very rapidly as $|m-n|$ becomes large.

Eigenvalues and eigenvectors of floquet operator

We use exact diagonalisation of the floquet evolution operator from equation (2.2.14) over one period. The eigenstates and eigenvalues are obtained.

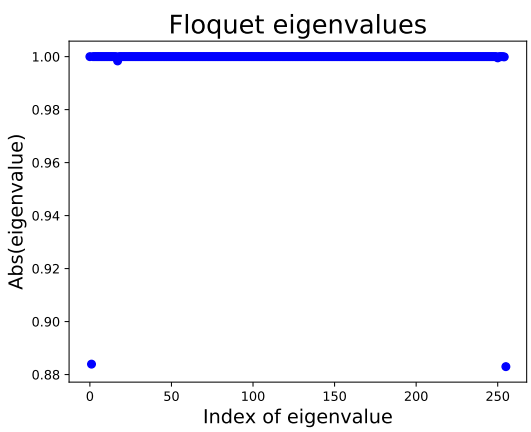

(a) K=1, basis= 256

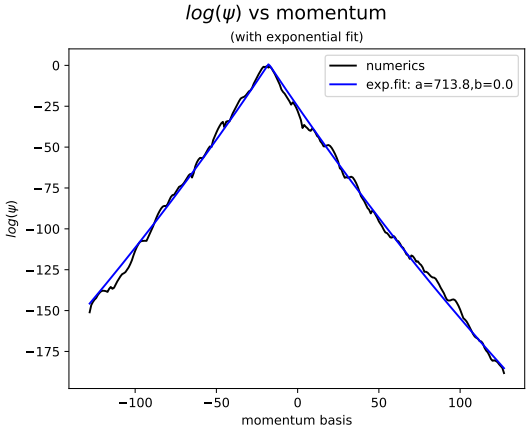

(b) K=1, basis= 256

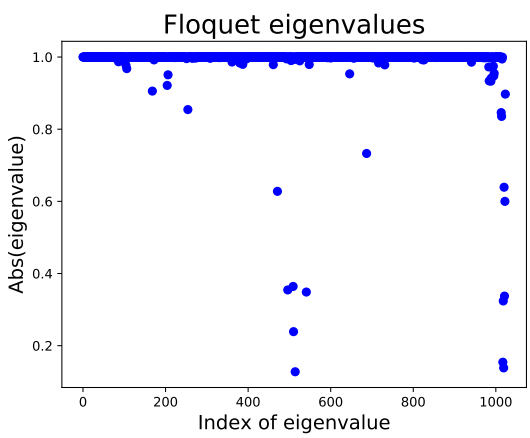

(c) K=8, basis= 1024

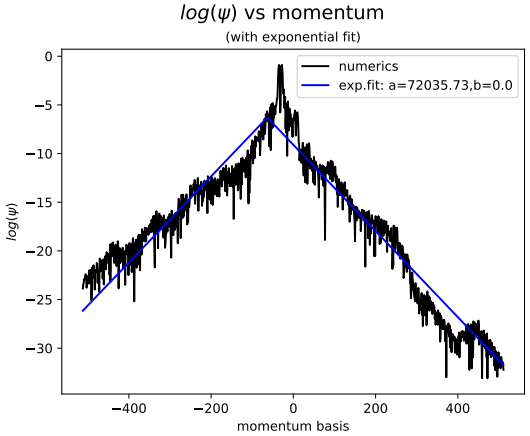

(d) K=8, basis= 1024

Figure 2.6: Eigenvalues and eigenvectors of tight binding impurity model (1d)

In the above figure 2.6 (a) and (c) the absolute values of eigenvalues of floquet operator are plotted for a given basis size, and in (b) and (d) a eigenvector of floquet operator is plotted in log scale.

As we see from the above plots the Eigenvectors ψ are exponentially localised. The floquet operator is unitary, so the Eigenspectrum should lie on a unit circle (Absolute value of eigenvalues is one). But due to truncation error, some of the eigenvalues lie inside the unit circle (Absolute value less than one). This error increase in increasing K.

Dynamics of Quantum Kicked Rotor

We have used the split evolution technique to get the time evolved wave functions of Kicked rotor and use exact diagonalisation to determine the spectral properties.

Split Evolution Technique

We have used first-order split evolution technique in our calculations, in which the operators in momentum and position space are acted on the wavefunction in their respective basis. The steps are mentioned below:

- Let's start with an initial state wave function which is a Gaussian wavefunction in momentum basis with a bandwidth W.

$$\phi_m(t=0) = Ae^{-\frac{(m-m_0)^2}{2W}} \tag{2.2.15}$$

where m_0 is the center of the Gaussian and the W variance of the Gaussian, which is also called the band width of the distribution and A is the normalisation constant.

- We evolve this wave function using the Floquet operator defined for the Kicked rotor Hamiltonian:

$$F(t) = e^{\frac{-iT_0(\hat{L})}{\hbar}} e^{\frac{-iV(\hat{\theta})}{\hbar}} \tag{2.2.16}$$

- The propagator is applied in two parts. First we start with wave function in the momentum space, and apply the free particle propagator $e^{\frac{-iT_0(\hat{L})}{\hbar}}$ to the wavefunction. This propagator is diagonal in momentum basis, so its straight forward to perform evolution.

- Now we transform the wavefunction in momentum basis to angle basis using the Fast Fourier Transform algorithm.

- Then the kick propagator $e^{\frac{-iV(\hat{\theta})}{\hbar}}$ is applied . In angle basis this propagator is diagonal, making the evolution trivial.

- Inverse Fast Fourier Transform (IFFT) is performed to transform the wavefunction back to momentum space. These above steps are repeated for every kick for t kicks.

- The wave function of the system after evolving for t kicks in momentum basis is $\phi_m(t)$ from $\phi_m(0)$. The expectation value of angular momentum ,

$$< \phi_m(t)|\hat{L^2}|\phi_m(t) > \equiv < L^2 > \tag{2.2.17}$$

  and the momentum density after t kicks is given by

$$|\phi_m(t)^2| \tag{2.2.18}$$

Dynamical localisation in quantum kicked rotor

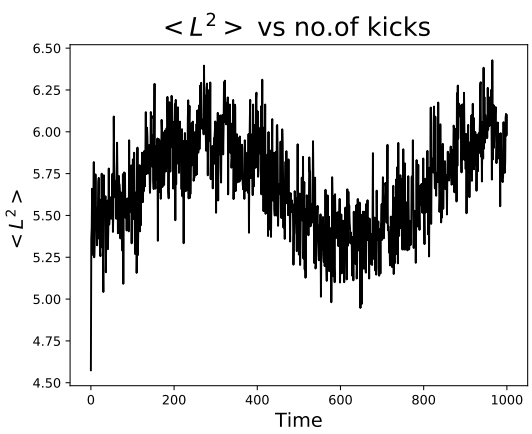

(a) K=1, basis size = 2048, time = 1000

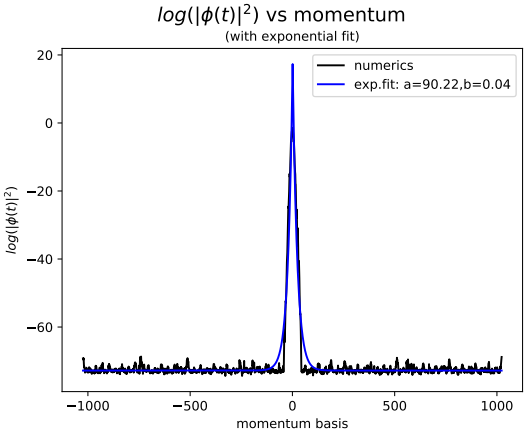

(b) K=1, basis size = 2048, time= 1000

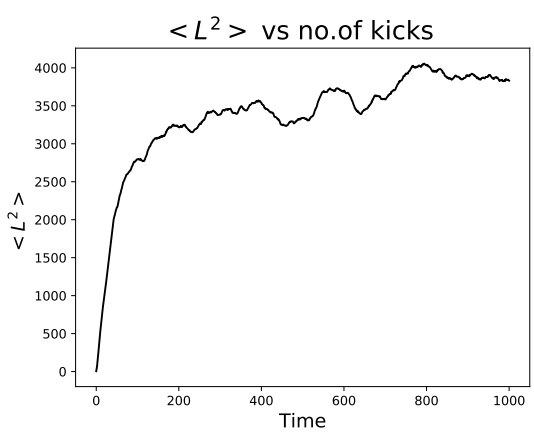

(c) K=8, basis size = 2048, time = 1000

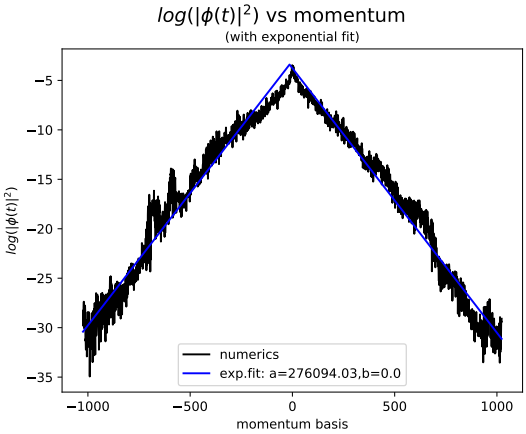

(d) K=8, basis size = 2048, time= 1000

Figure 2.7: Dynamics of Quantum kicked rotor

In the above figures 2.7 (a) and (c) $< L^2 >$ is plotted versus time and (b) and (d) the final momentum density: $|\phi_m(t)^2|$ is plotted in log scale versus momentum basis after $t = 1000$ kicks, for effective plank constant of the system $\alpha = \hbar = 1$. The exponential fit it the final momentum density plot is of the form: $a\exp(-b|m|)$, m represents momentum space.

The $< L^2 >$ vs time plot shows localized behaviour for large time and the $log(|\phi_m(t)|^2)$ vs momentum basis plot also implies exponential localisation of evolved wavefunction in momentum space, this behaviour is called dynamical localisation. On increasing the kick strength the localisation length increases in momentum space.

2.3 Varying effective $\hbar$ of the system

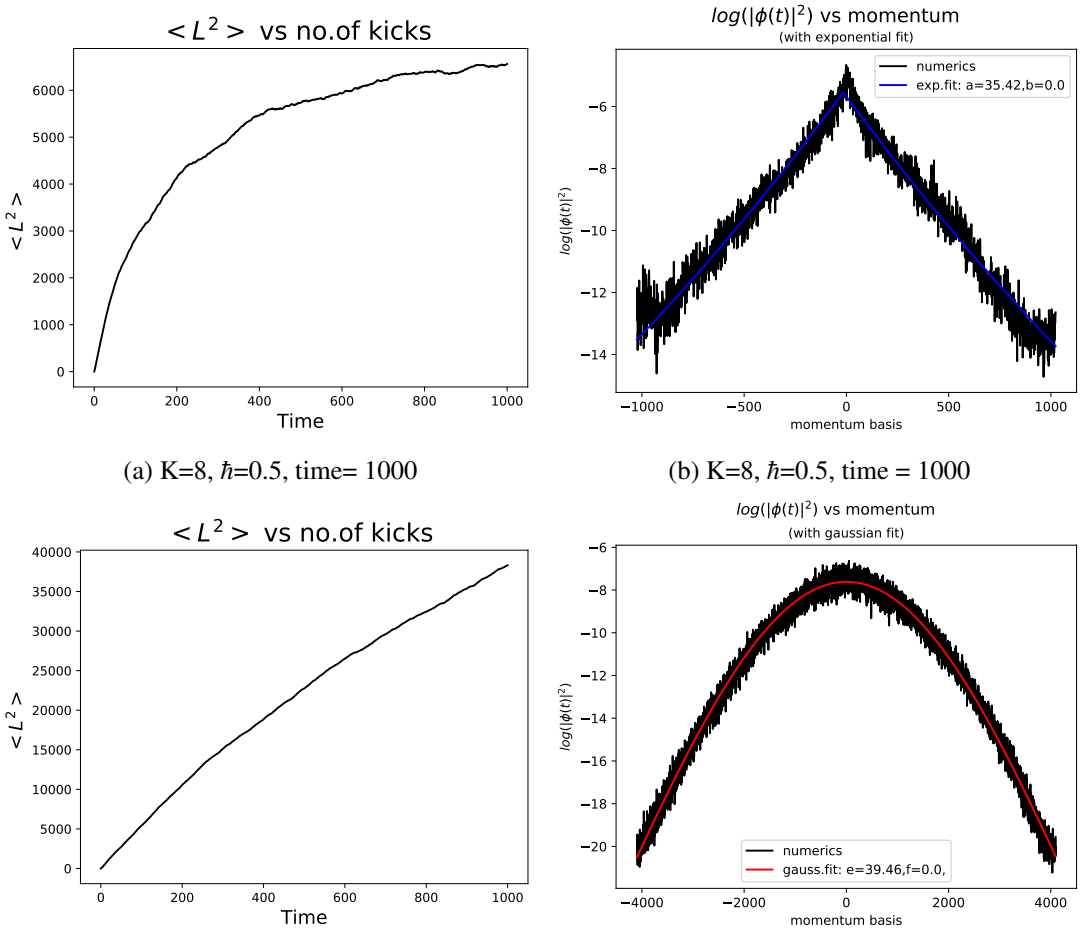

(a) K=8, $\hbar$=0.5, time= 1000

(b) K=8, $\hbar$=0.5, time = 1000

(c) K=8, $\hbar$=0.1, time= 1000

(d) K=8, $\hbar$=0.1, time=1000

Figure 2.8: Dynamics of QKR with smaller effective $\hbar$

In the above figures 2.8 (a) and (c) $< L^2 >$ is plotted versus time for effective planks constant $\hbar = 0.5$ and $\hbar = 0.1$. The final momentum density after 1000 kicks is plotted in log scale ($\log|\phi(t)|^2$) versus momentum basis for $\hbar = 0.5$ in (b) and for $\hbar = 0.1$ in (d) respectively. The exponential fit it the final momentum density plot is of the form: $a\exp(-b|m|)$ and Gaussian fit is of the form : $e\exp(\frac{-m^2}{2f})$

It's seen the property of localisation is destroyed on decreasing $\hbar$. One has to be careful here as to obtain the above-shown dynamics the time taken (break time) should be increased and also momentum basis size should be increased to avoid boundary effects.

The break time (τ_b) is defined as the approximate time we need to evolve the system to observe dynamical localisation. Break time increases on decreasing the $\hbar$ of the system.

$$\tau_b \approx \frac{K^2}{\hbar^2} \tag{2.3.1}$$

From the figures 2.8 (b) and (d), we can see that how the best fit for $log(|\phi^2(t)|)$ changes from exponential to Gaussian on decreasing the effective $\hbar$ of the system. As $\hbar$ tends to zero the quantum kicked rotor shows classical behaviour.

2.4 Noise in kicking strength

Noise (ε) has been added on the kicking strength for every kick, such that for every kick the kicking strength is drawn from uniformly distribution from $[K-\varepsilon, K+\varepsilon]$.

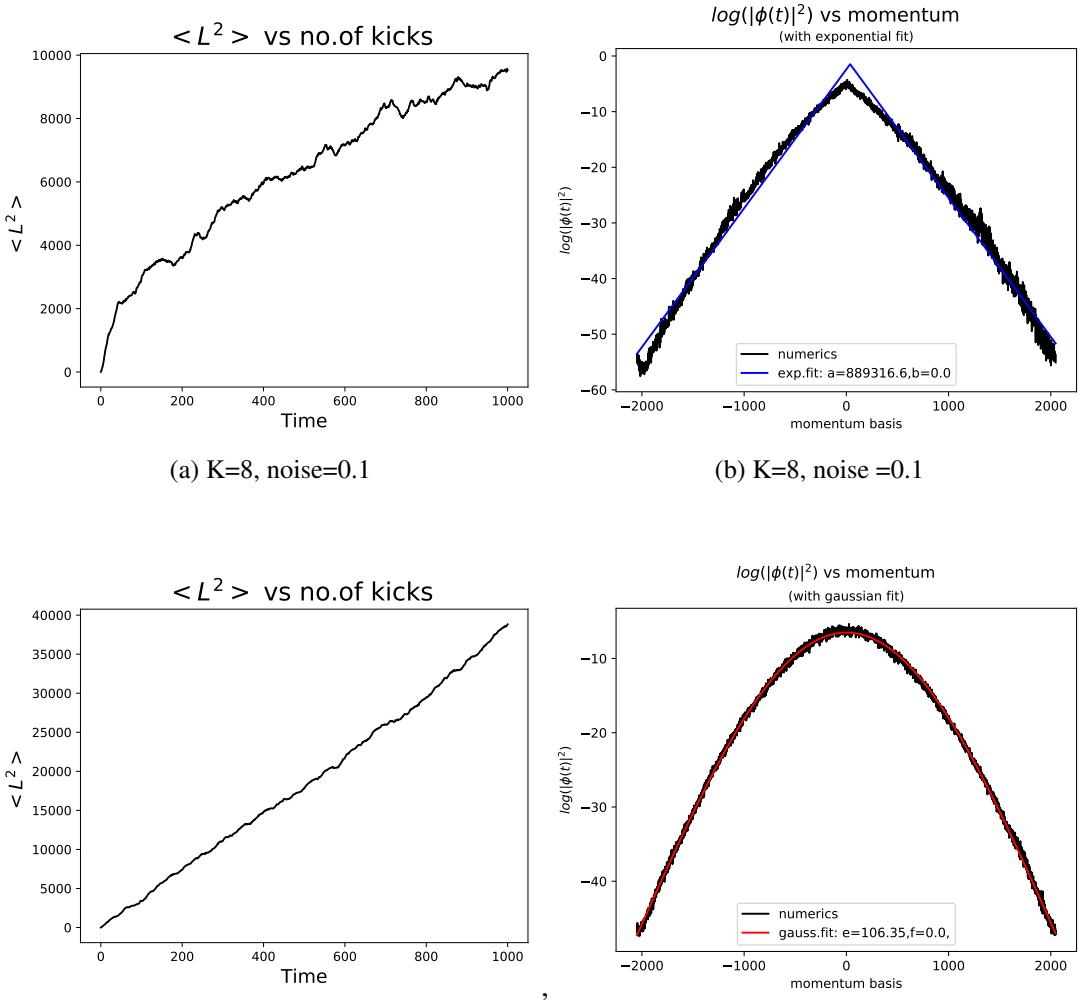

(a) K=8, noise=0.1

(b) K=8, noise =0.1

(c) K=8, noise=0.5

(d) K=8, noise = 0.5

Figure 2.9: Dynamics of QKR with noise in kicks.

In the above figure 2.9, the behaviour of $< L^2 >$ vs time and final momentum density after 1000 kicks in log scale ($log(|\phi(t)|^2)$) is plotted for quantum kicked rotor with noise in kicking. To experimentally realise dynamical localization in kicked rotor via cold atoms the noise in the kick strength during every kick should be significantly low.

On introducing the noise in kicking the dynamical localisation in momentum space is destroyed and the dynamics become completely diffusive for sufficient noise in kicking.

2.5 Mapping kicked rotor to 1d tight binding impurity model

In this section, we explain the mapping between a kicked rotor and a 1d Anderson-type model [9]

Due to the presence of the discrete-time translation symmetry in the Hamiltonian, floquet theory implies the existence of a conserved quantity called quasi-energy(ω). The quasi-energy states have the below mentioned form

$$\phi_\omega(\theta,t) = e^{-\imath\omega t} u_\omega(\theta,t) \tag{2.5.1}$$

where $u_\omega(\theta,t+1) = u_\omega(\theta,t)$.

States with different quasi-energies are orthogonal. The unitary evolution operators, in this case, turn out to be the floquet operators.

$$F = e^{-\frac{\imath V(\theta)}{\hbar}} e^{-\frac{\imath T(n)}{\hbar}} \tag{2.5.2}$$

Where $T(n)$ is the kinetic energy operator and $V(\theta)$ is the potential energy operator of kicked rotor.

Time evolution using floquet operators is given by :

$$|\phi_\omega(t+1)\rangle = F\,|\phi_\omega(t)\rangle \tag{2.5.3}$$

Similarly, we define $u_n^{\pm}$ as the angular momentum representation of the state just before and after a kick.

$$u_n^{\pm} = \frac{1}{\sqrt{2\pi}} \int_0^{2\pi} d\theta e^{-in\theta} u^{\pm}(\theta) \tag{2.5.4}$$

Between the kicks, the evolution is simple

$$u_m^- = e^{\imath\omega} e^{-\imath T(n)} u_m^+ \tag{2.5.5}$$

For determining the effect of the kick, it is better to return to the angle representation

$$u^+(\theta) = e^{-\imath V(\theta)} u^-(\theta) \tag{2.5.6}$$

Combining the above two equations (2.5.6) and (2.5.5), we get

$$u_m^+ = e^{\imath\omega} \sum_n J_{m-n} e^{-\imath\hbar n^2/2} u_n^+ \tag{2.5.7}$$

where J_{m-n} is the Bessel function of first kind.

we define the following quantities :

$$|\overline{u}(\theta)\rangle := \left(\left|u^{+}(\theta)\right\rangle + \left|u^{-}(\theta)\right\rangle\right)/2 \tag{2.5.8}$$

$$W := -\tan\left(\frac{V(\theta)}{2}\right) \tag{2.5.9}$$

Rewriting equation (2.5.6) in terms of $\overline{u}(\theta)$we get

$$u^{-}(\theta) = \overline{u}(\theta)(1-\imath W(\theta)) \tag{2.5.10}$$

$$u^{+}(\theta) = \overline{u}(\theta)(1+\imath W(\theta)) \tag{2.5.11}$$

the Fourier Transform of the above equations:

$$u_m^{-} = \frac{1}{\sqrt{2\pi}}\int_0^{2\pi} d\theta e^{-im\theta}\overline{u}(\theta)(1-\imath W(\theta)) \tag{2.5.12}$$

$$u_m^{+} = \frac{1}{\sqrt{2\pi}}\int_0^{2\pi} d\theta e^{-im\theta}\overline{u}(\theta)(1+\imath W(\theta)) \tag{2.5.13}$$

Where $\overline{u}_n$ is the nth Fourier component of $\overline{u}(\theta)$, and W_n is the nth Fourier component of $W(\theta)$. For simplicity, we use u to stand for $\overline{u}$.

$$u_m - \imath\sum_r W_r u_{m+r} = e^{\imath E_m}\left(u_m + \imath\sum_r W_r u_{m+r}\right) \tag{2.5.14}$$

here

$$E_m := \omega - T(m) \tag{2.5.15}$$

Next we isolate the term $r=0$ in each sum to one side, and rewrite the equation, we obtain

$$T_m u_m + \sum_{r\neq 0} W_r u_{m+r} = E u_m \tag{2.5.16}$$

This the tight-binding model obtained in the momentum space it has a structure similar to the Anderson impurity model. The onsite potential (T_m) is quasi-random and the hopping strength (W_r) is short-ranged [9].

In the above equation (2.5.16)

$$E := -W_0 \tag{2.5.17}$$

$$T_m := \iota \frac{1 - e^{\iota\left(\omega - m^2/2\right)}}{1 + e^{\iota(\omega - m^2/2}} = \tan\left(\frac{E_m}{2}\right) \tag{2.5.18}$$

Similarity between QKR and Tight binding model

Kicked rotor	Tight binding model(Anderson)
$T(m)$: kinetic energy $\tan([\omega - T(m)]/2)$	T_m : On-site potential
$V(\theta)$: potential $-\frac{1}{\sqrt{2\pi}} \int_0^{2\pi} d\theta e^{-ir\theta} \tan[V(\theta)/2]$	W_r : Hopping potential
Angular momentum (m)	Lattice sites (r)

From Feynman -Hellman theorem we find that

$$dE/d\omega = \sum \frac{\left\langle \sec^2 E_m \right\rangle}{2} \geq 0 \tag{2.5.19}$$

The above equation implies E is monotonic function of ω. The characteristic of Eigenspectrum and wave function is same in both the pictures.

Average IPR

For a single eigenstate ϕ_α, the IPR is defined as

$$IPR_\alpha = \sum_{\mathbf{m}} | < \mathbf{m} | \phi_\alpha >^4 | \tag{2.5.20}$$

where $|\mathbf{m}>$ is the momentum basis state.

The average IPR over the eigenstates in the truncated Hilbert space of d dimension with linear size L.

$$< IPR >= \frac{\sum_\alpha IPR_\alpha}{L^d} \tag{2.5.21}$$

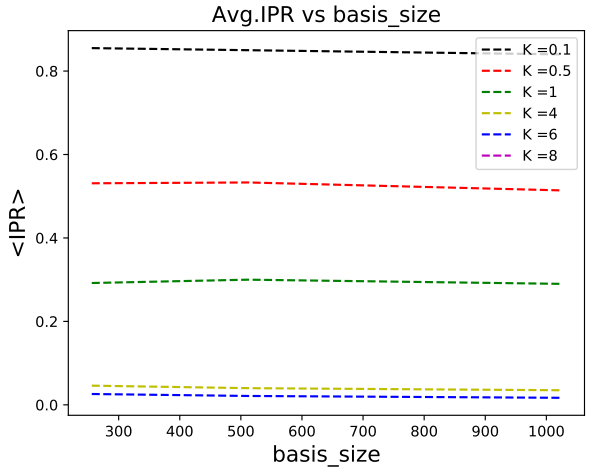

Figure 2.10: Average IPR vs system size (1d)

In the above figure 2.10 the average IPR of the eigenstates is plotted versus linear system size (L) for various values of kick strength (K) in the mapped 1d tight binding lattice (2.5.16) .

Its clearly seen that the Average IPR doesn't scale with the basis size for any value of kicking strength implying the the localised nature of eigenstates.

Average Level spacing ratio

To check the properties of system like integrability and ergodicity, Average level spacing ratio is a good measure, its defined as:

$$\langle r \rangle = \frac{1}{L^d - 2} \sum_{\alpha=1}^{L^d-2} \frac{\min\{\gamma_\alpha, \gamma_{\alpha+1}\}}{\max\{\gamma_\alpha, \gamma_{\alpha+1}\}} \tag{2.5.22}$$

where, $\gamma_\alpha = \omega_{\alpha+1} - \omega_\alpha$, ω_α are the eigenvalues, L is the linear system size and d is the dimension of the lattice.

The level spacing distribution can be found with the help of average level spacing ratios $< r >$ [22]:

if $< r >$ = 0.386 then the level spacing distribution is Poisson and the system is integrable

if $< r >$ = 0.530 the level spacing distribution is Wigner Dyson and the system is ergodic.

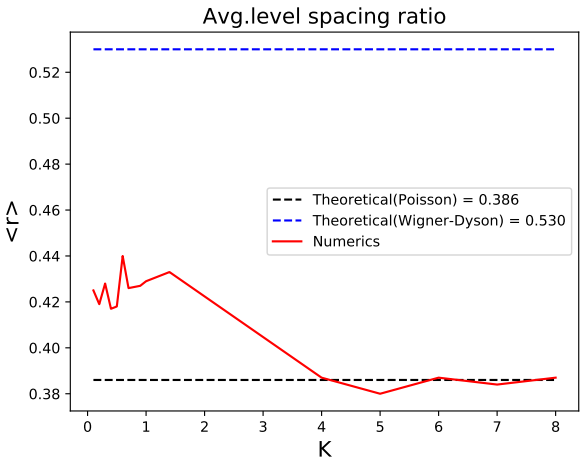

Figure 2.11: Average Level spacing ratio vs K (1d)

In the above figure, 2.11 the average level spacing ratio is plotted versus the kick strength (K).

The Average level spacing ratio lies near 0.386 implying the level spacing distribution follows a Poisson distribution, a signature of dynamical localisation in the system.

3 Two spatially Coupled kicked rotors

In this chapter, we are going to study the dynamics of Two kicked rotors which are coupled spatially with a nonlinear coupling of the form $\cos(\theta_1+\theta_2)$ with a coupling strength. We are going to investigate how this interaction in kicks can modify the properties of the kicked rotor discussed in the previous chapter.

Hamiltonian of coupled kicked rotor

$$H=\frac{L_1^2}{2}+\frac{L_2^2}{2}+[K_1\cos(\theta_1)+K_2\cos(\theta_2)+J\cos(\theta_1+\theta_2)]\sum_{n=-\infty}^{+\infty}\delta(t-n) \tag{3.0.1}$$

K_1, K_2 are the strengths of kicking and J is the coupling strength.

3.1 Two spatially coupled classical kicked rotor

Equations of motion are obtained from canonical equations of motion are:

$$\dot{\theta}_i=\frac{\partial H}{\partial L_i}\quad \dot{L}_i=-\frac{\partial H}{\partial \theta_i} \tag{3.1.1}$$

where i=1,2.

$$L_{n+1}^{(1)}=L_n^{(1)}+K_1\sin\theta_n^{(1)}+J\sin\left(\theta_n^{(1)}+\theta_n^{(2)}\right) \tag{3.1.2}$$

$$L_{n+1}^{(2)}=L_n^{(2)}+K_2\sin\theta_n^{(2)}+J\sin\left(\theta_n^{(1)}+\theta_n^{(2)}\right) \tag{3.1.3}$$

$$\theta_{n+1}^{(1)}=\theta_n^{(1)}+L_{n+1}^{(1)} \tag{3.1.4}$$

$$\theta_{n+1}^{(2)}=\theta_n^{(2)}+L_{n+1}^{(2)} \tag{3.1.5}$$

Diffusion constant for classical coupled kicked rotor

We have obtained a first-order approximation to the classical diffusion constant similar to the kicked rotor by assuming a uniform probability distribution for the angle, and integrating over this distribution.

$$D^{(1)} = \frac{1}{4\pi^2}\int_0^{2\pi}\left(L_{n+1}^{(1)} - L_n^{(1)}\right)^2 d\theta_n^{(1)} d\theta_n^{(2)} \tag{3.1.6}$$

$$D^{(1)} = \frac{1}{4\pi^2}\int_0^{2\pi} d\theta_n^{(1)} d\theta_n^{(2)} \left[K_1 \sin\theta_n^{(1)} + J_1 \sin(\theta_n^{(1)} + \theta_n^{(2)})\right]^2 \tag{3.1.7}$$

$$D^{(1)} = \frac{K_1^2}{2} + \frac{J^2}{2} \tag{3.1.8}$$

Similarly

$$D^{(2)} = \frac{K_2^2}{2} + \frac{J^2}{2} \tag{3.1.9}$$

Average energy along two different directions is given by:

$$< E_1 >= \frac{< L_1^2 >}{2} = D^{(1)} t \tag{3.1.10}$$

$$< E_2 >= \frac{< L_2^2 >}{2} = D^{(2)} t \tag{3.1.11}$$

Plots of Two classical coupled kicked rotor

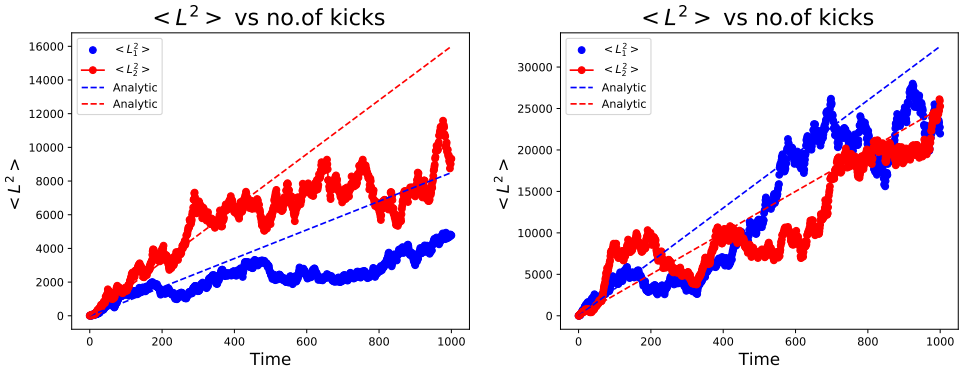

(a) K_1=1, K_2=4,J=1 (b) K_1=8, K_2=7,J=1

Figure 3.1: $< L^2 >$ vs time for classical coupled kicked rotor

From the above figure 3.1 $< L^2 >$ vs time plots, shows that for large values of kick strengths the dynamics is diffusive

Analytically calculated diffusion constant fits quite well with the slope of $< L^2 >$ vs time for large values of kick strength ($K_1, K_2 >> 1$) as the first-order approximation used to calculate the diffusion constant is valid only when the phase space is the completely chaotic.

3.2 Two spatially coupled quantum kicked rotor

The quantum operators corresponding to L_1 and L_2 are $\hat{L}_1 = -\imath\partial/\partial\theta_1$ and $\hat{L}_2 = -\imath\partial/\partial\theta_2$ respectively. Like the one-dimensional case studied in the previous chapter, we have the Floquet-operator .

$$\hat{F} = e^{\frac{-\imath V(\hat{\theta_1},\theta_2)}{\hbar}} e^{-\frac{\imath T(\hat{L}_1,\hat{L}_2)}{\hbar}} \tag{3.2.1}$$

We construct dimensionless parameters α and β, they are defined as follows:

$$\alpha_{1,2} := \frac{\hbar T}{I_{1,2}}$$

$$\beta_{1,2} = \frac{K_{1,2}}{\hbar}, \beta_3 = \frac{J}{\hbar}$$

are dimensionless kicking and coupling strengths.

In all our calculation $T = I = 1$

$$\alpha_{1,2} = \hbar$$

$$\beta_{1,2} = \frac{K_{1,2}}{\hbar}, \beta_3 = \frac{J}{\hbar}$$

We use a split operator technique to perform time evolution. The split operators act on an initial wavefunction, and the evolved wavefunction is used to compute $< L^2 >$ and momentum density($|\phi_{\mathbf{m}}(t)|^2$)

Here $\mathbf{m} = (m_1, m_2)$ represents the momentum basis states.

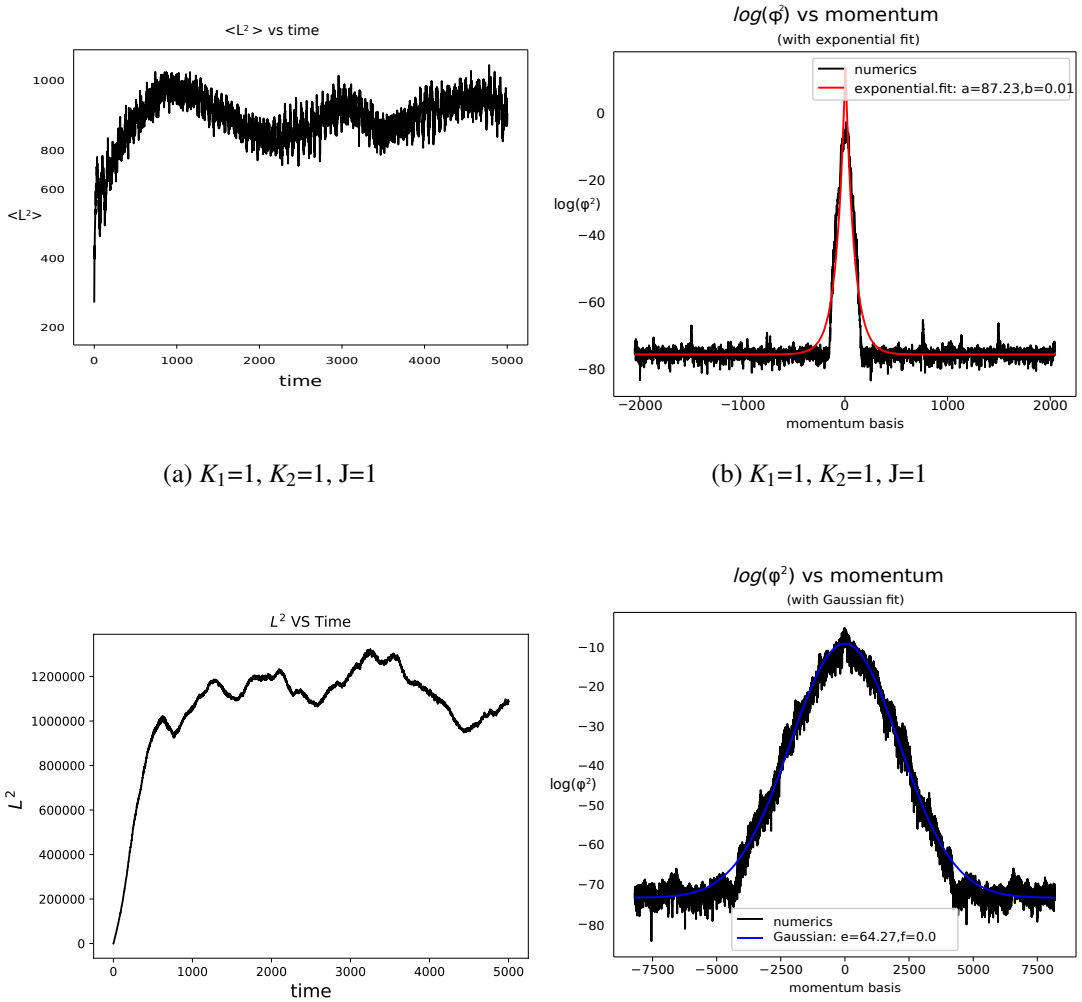

(a) K_1=1, K_2=1, J=1

(b) K_1=1, K_2=1, J=1

(c) K_1=1, K_2=1, J=8

(d) K_1=1, K_2=1, J=8

Figure 3.2: Dynamics of two spatially coupled quantum kicked rotor

In the above figure 3.2 $< L^2 >$ vs time in one direction and the final momentum density after time evolution of 5000 kicks in a log scale ($|\phi(t)^2|$) are plotted for a two spatially coupled quantum kicked rotor system. The exponential fit of the final momentum density plot is of the form: $a\exp(-b|m|)$ and Gaussian fit is of the form : $e\exp(\frac{-m^2}{2f})$

We observe that on increasing the coupling strength the break-time increases to observe dynamical localisation. The density profile in a log scale plot has an exponential fit but on increasing the coupling strength the best fit becomes a Gaussian. The high coupling strength limit of two coupled quantum kicked rotor has some similarity with the weak localisation limit in 2d Anderson model.

3.3 Mapping Two Coupled Kicked rotor to 2d tight binding impurity model

Due to the presence of discrete-time invariance in the Hamiltonian, using Floquet Bloch theorem the eigenstates will be the form.

$$\psi_\omega = e^{-\iota\omega t} u_\omega(\theta_1, \theta_2, t) \tag{3.3.1}$$

Here $T\left(\hat{L}_1, \hat{L}_2\right) = \frac{1}{2}\hat{L}_1^2 + \frac{1}{2}\hat{L}_2^2$ are the kinetic energy terms in the Hamiltonian. $\hat{V}(\theta_1, \theta_2)$ denotes the potential energy terms.

The eigenvectors are given by

$$u_{\mathbf{m}} := \langle m_1 m_2 | \overline{u} \rangle$$

$(\mathbf{m}) \equiv (m_1, m_2)$ is a two dimensional basis vector.

$$u_{\mathbf{m}} = \int_0^{2\pi} \frac{d\theta_1 d\theta_2}{2\pi} e^{-\iota(m_1\theta_1 + m_2\theta_2)} \overline{u}(\theta_1, \theta_2) \tag{3.3.2}$$

Here $|\overline{u}(\theta_1, \theta_2)\rangle = (|u^+\rangle + |u^-\rangle)/2$

Following the same arguments as in the 1d case, we arrive at the tight-binding model on the two-dimensional Anderson lattice

$$T_{\mathbf{m}} u_{\mathbf{m}} + \sum_{\mathbf{r}\neq 0} W_{\mathbf{r}} u_{\mathbf{m}+\mathbf{r}} = E u_{\mathbf{m}} \tag{3.3.3}$$

Onsite potential is given by

$$T_{\mathbf{m}} := \tan\left([\omega - T(\mathbf{m})]/2\right) \tag{3.3.4}$$

Kinetic energy

$$T(\mathbf{m}) := \frac{1}{2}\left(\alpha_1 m_1^2 + \alpha_2 m_2^2\right) \tag{3.3.5}$$

$$W(\theta_1, \theta_2) = \tan\left[V(\theta_1, \theta_2)/2\right] \tag{3.3.6}$$

Hopping term in momentum space

$$W_{\mathbf{r}} = \int_0^{2\pi} \frac{d\theta_1 d\theta_2}{2\pi} e^{-\iota(r_1\theta_1 + r_2\theta_2)} W(\theta_1, \theta_2) \tag{3.3.7}$$

$$E := -W_0 \tag{3.3.8}$$

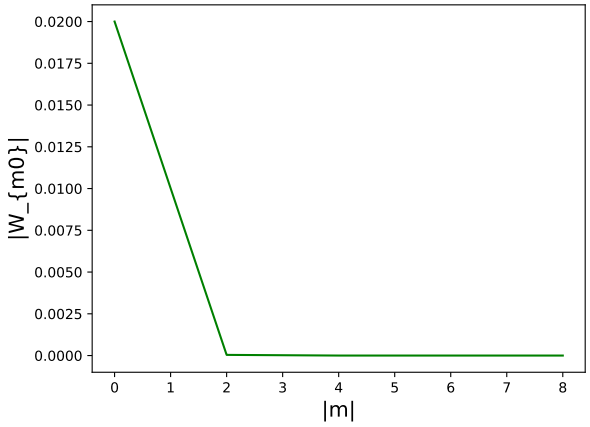

Figure 3.3: Modulus of hopping in tight binding impurity model (2d)

In the above figure3.3 Hopping term $|W_{\mathbf{m0}}|$ of 2d mapped tight-binding lattice is plotted with lattice distance in momentum space. From this above plot, we can conclude that the hopping in 2d mapped lattice is short-ranged, justifying the name tight binding to the lattice.

Average IPR of mapped 2d tight-binding lattice

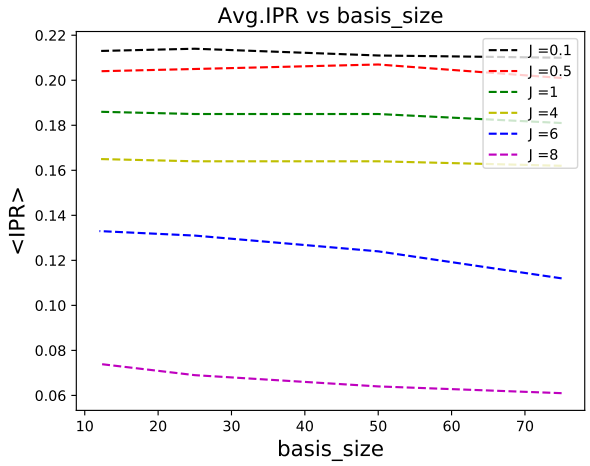

Figure 3.4: Average IPR vs system size (2d)

The average IPR is averaged IPR over all the eigenstates. The average IPR is plotted with linear size of the system for the mapped 2d lattice Hamiltonian from equation (3.3.3) for varying coupling strength (J) and for fixed kick strengths $K_1 = K_2 = 1$ in figure 3.4 .

The average IPR $\to 0$ slowly for high values of coupling ($J \geq 4$) as the system size is increased, this might be signature of weak localisation in coupled kicked rotor similar to 2d Anderson model. But for lower values of coupling strengths ($J \leq 1$), the average IPR seems to be constant with system size

implying the localised nature of eigenstates.

Average Level spacing ratio of mapped 2d lattice Hamiltonian

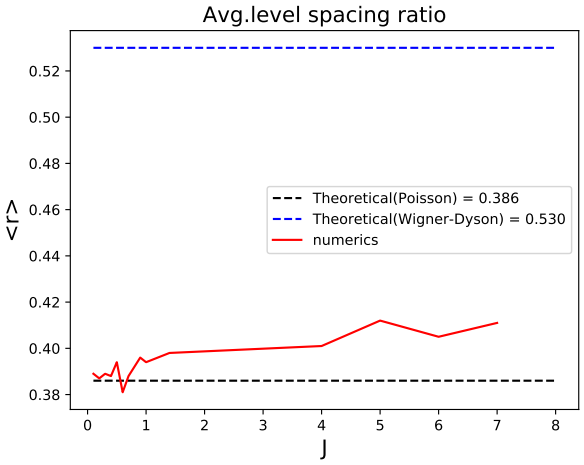

Figure 3.5: Average Level spacing ratio vs J (2d)

In the above figure 3.5 the average level spacing ratio is plotted versus the coupling strength (J).

The average level spacing ratio is the level spacing ratio average overall eigenvalues of the system. From the figure 3.5 in which average level spacing ratio vs coupling strength (J) is plotted, it's seen that that for small coupling strengths the dynamics is localised ($< r > \approx 0.386$) implying the presence of dynamical localisation. But for high values of coupling strength ($J \geq 4$) the average level spacing ratio is $< r > \approx 0.41$ this deviation might be the signature of weak localisation.

4 Three spatially coupled kicked rotor

In this chapter, we are going to study the dynamics of Three kicked rotors which are coupled spatially with a nonlinear nearest neighbour coupling of the form $\cos(\theta_i + \theta_j)$ with a coupling strength. We are going to investigate how this interaction in kicks can modify the properties compared to that of the kicked rotor and two coupled kicked rotors discussed in the previous chapters.

Hamiltonian of the system is

$$H = \frac{1}{2}L_1^2 + \frac{1}{2}L_2^2 + \frac{1}{2}L_3^2 + [\sum_{i=1}^{3} K_i \cos\theta_i + J\sum_{i\neq j}\cos(\theta_i + \theta_j)] \sum_{n=-\infty}^{+\infty} \delta(t-n) \tag{4.0.1}$$

Where K_1, K_2, K_3 are the kicking strengths and J is the coupling strength between the rotors.

4.1 Three Classical coupled Kicked rotor

Equations of motion are obtained from canonical equations

$$\dot{\theta}_i = \frac{\partial H}{\partial L_i} \quad \dot{L}_i = -\frac{\partial H}{\partial \theta_i} \tag{4.1.1}$$

where i=1,2,3

$$L_{n+1}^{(1)} = L_n^{(1)} + K_1 \sin\theta_n^{(1)} + J[\sin\left(\theta_n^{(1)} + \theta_n^{(2)}\right) + \sin\left(\theta_n^{(1)} + \theta_n^{(3)}\right)] \tag{4.1.2}$$

$$L_{n+1}^{(2)} = L_n^{(2)} + K_2 \sin\theta_n^{(2)} + J[\sin\left(\theta_n^{(2)} + \theta_n^{(1)}\right) + \sin\left(\theta_n^{(2)} + \theta_n^{(3)}\right)] \tag{4.1.3}$$

$$L_{n+1}^{(3)} = L_n^{(3)} + K_3 \sin\theta_n^{(3)} + J[\sin\left(\theta_n^{(3)} + \theta_n^{(1)}\right) + \sin\left(\theta_n^{(3)} + \theta_n^{(2)}\right)] \tag{4.1.4}$$

$$\theta_{n+1}^{(1)} = \theta_n^{(1)} + L_{n+1}^{(1)} \tag{4.1.5}$$

$$\theta_{n+1}^{(2)} = \theta_n^{(2)} + L_{n+1}^{(2)} \tag{4.1.6}$$

$$\theta_{n+1}^{(3)} = \theta_n^{(3)} + L_{n+1}^{(3)} \tag{4.1.7}$$

Diffusion constant for three spatially coupled kicked rotors

$$D^{(1)} = \frac{K_1^2}{2} + J^2 \tag{4.1.8}$$

$$D^{(2)} = \frac{K_2^2}{2} + J^2 \tag{4.1.9}$$

$$D^{(3)} = \frac{K_3^2}{2} + J^2 \tag{4.1.10}$$

Average energy along three different directions is given by:

$$< E_1 >= \frac{< L_1^2 >}{2} = D^{(1)} t \tag{4.1.11}$$

$$< E_2 >= \frac{< L_2^2 >}{2} = D^{(2)} t \tag{4.1.12}$$

$$< E_3 >= \frac{< L_3^2 >}{2} = D^{(3)} t \tag{4.1.13}$$

Plots of three classical coupled KR

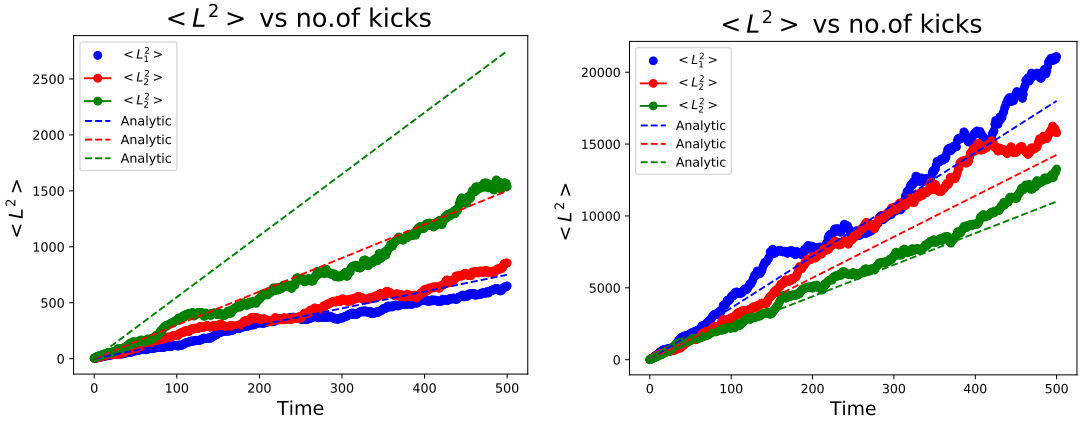

(a) $K_1 = 1, K_2 = 2, K_3 = 3, J = 1$ (b) $K_1 = 8, K_2 = 9, K_3 = 10, J = 2$

Figure 4.1: $< L^2 >$ vs time for three classical spatially coupled kicked rotor

In the above figure 4.1 $< L^2 >$ is plotted versus time for small(a) and large(b) values of kick strength along with an analytically calculated fit from equation (4.1.11).

This first-order approximation of diffusion constant is a good approximation with the numerically calculated values of $< L^2 >$ in the plots with large kick strengths (b). But in the case of small kick strengths, the analytic fit is not good, this implies the presence of regular regions in classical phase space and this regime first-order approximation to calculate diffusion constants doesn't hold good.

4.2 Three Coupled Quantum Kicked rotors

The quantum operators corresponding to L_1, L_2 and L_3 are $\hat{L}_1 = -\iota\partial/\partial\theta_1$, $\hat{L}_2 = -\iota\partial/\partial\theta_2$ and $\hat{L}_3 = -\iota\partial/\partial\theta_3$ respectively. Like the one-dimensional case studied in the previous chapter, we have a Floquet-operator of similar form.

$$\hat{F} = e^{\frac{-\iota V(\theta_1,\hat{\theta}_2,\theta_3)}{\hbar}} e^{-\frac{\iota T(\hat{L}_1,\hat{L}_2,\hat{L}_3)}{\hbar}} \tag{4.2.1}$$

We construct dimensionless parameters of the system similar to the one constructed in the previous chapter.

$$\alpha_{1,2,3} := \frac{\hbar T}{I_{1,2,3}}$$

$$\beta_{1,2,3} = \frac{K_{1,2,3}}{\hbar}, \beta_4 = \frac{J}{\hbar}$$

are dimensionless kicking and coupling strengths .

In all our calculation $T = I = 1$ so,

$$\alpha_{1,2,3} = \hbar$$

$$\beta_{1,2,3} = \frac{K_{1,2,3}}{\hbar}, \beta_4 = \frac{J}{\hbar}$$

We use a split operator technique to perform time evolution. Using this technique we evolve the initial wavefunction, and the evolved wavefunction is used to determine $< L^2 >$ along any direction and final momentum density $|\phi_{\mathbf{m}}(t)|^2$.

Here $\mathbf{m} = (m_1, m_2, m_3)$ is the representation of momentum basis states.

Dynamics of three coupled quantum kicked rotors

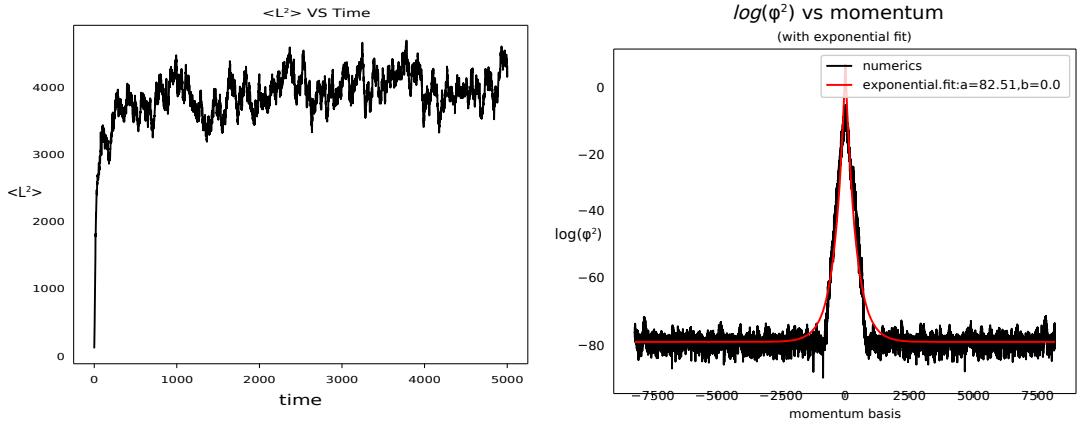

(a) K_1=K_2=K_3=1,J=0.5

(b) K_1=K_2=K_3=1,J=0.5

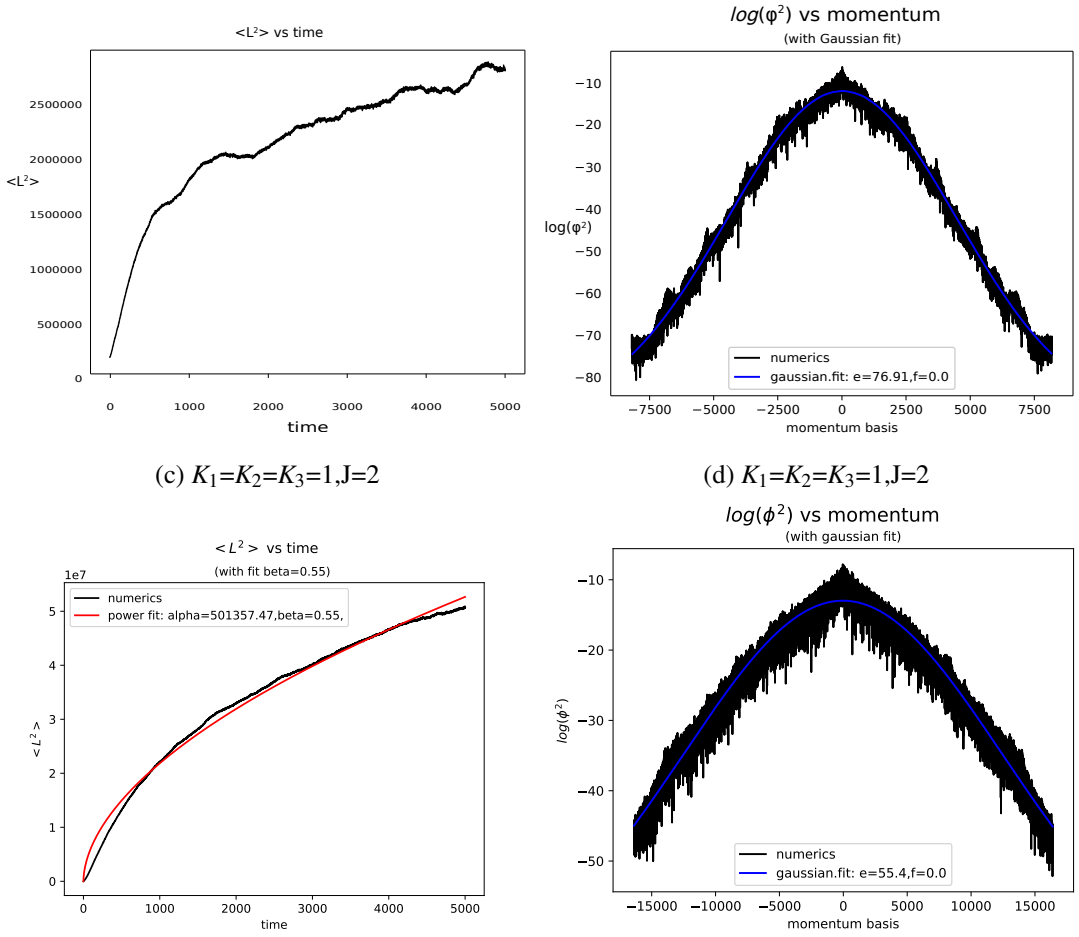

(c) K_1=K_2=K_3=1,J=2

(d) K_1=K_2=K_3=1,J=2

(e) K_1=K_2=K_3=1,J=4

(f) K_1=K_2=K_3=1,J=4

Figure 4.2: Dynamics of three spatially coupled kicked rotors

In the above figure 4.2 $< L^2 >$ vs time along one direction is plotted in (a),(c),(e) and final momentum density $|\phi_{\mathbf{m}}(t)|^2$ after 5000 kicks (b),(d),(f) is plotted in log scale for three spatially coupled kicked rotors.

For small values of kick strength, the dynamics is localised in momentum space but on increasing the kick strength the localisation in destroyed. To make sure the saturation in energy is only due to quantum effects not due to boundary effects we need to evolve the wavefunction for a long time and take a larger momentum basis to capture the full dynamics. For large values of kick strength ($J \geq 4$) the dynamics is quasi-diffusive ($< L^2 > \approx t^{\beta}$) where $0 \leq \beta \leq 1$.

This implies that there is a transition from dynamical localised to dynamical delocalized phase on increasing the coupling strength of the kicked rotor.

4.3 Mapping Three Coupled Kicked rotor to 3d tight binding impurity model

Using similar arguments as used for Two coupled kicked rotor its straight forward to map Three coupled kicked rotor model to a 3d tight biding model.

$$T_{\mathbf{m}} u_{\mathbf{m}} + \sum_{\mathbf{r}\neq 0} W_{\mathbf{r}} u_{\mathbf{m}+\mathbf{r}} = E u_{\mathbf{m}} \tag{4.3.1}$$

Here, $(\mathbf{m}) \equiv (m_1, m_2, m_3)$ is the representation of momentum basis states.

The onsite potential has the form

$$T_{\mathbf{m}} := \tan\left(\left[\omega - E_{\mathbf{m}}\right]/2\right) \tag{4.3.2}$$

where

$$E_{\mathbf{m}} := \frac{1}{2}\left(\alpha_1 m_1^2 + \alpha_2 m_2^2 + \alpha_3 m_3^2\right) \tag{4.3.3}$$

The hopping matrix elements in momentum space is given by:

$$W_{\mathbf{r}} = \int_0^{2\pi} \frac{d\theta_1 d\theta_2 d\theta_3}{2\pi} e^{-\imath(r_1\theta_1 + r_2\theta_2 + r_3\theta_3)} W\left(\theta_1, \theta_2, \theta_3\right) \tag{4.3.4}$$

$$W\left(\theta_1, \theta_2, \theta_3\right) = \tan\left[V\left(\theta_1, \theta_2, \theta_3\right)/2\right] \tag{4.3.5}$$

$$E := -W_0 \tag{4.3.6}$$

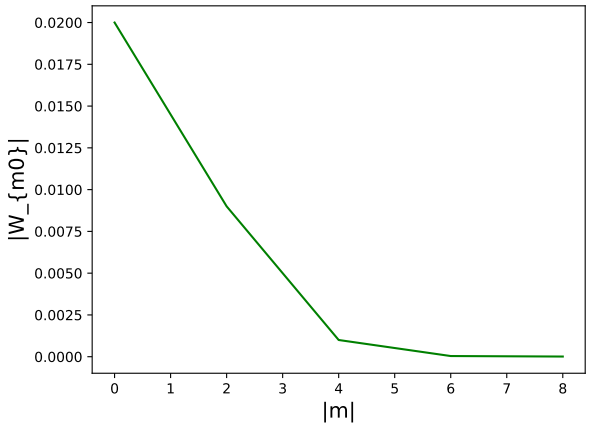

Figure 4.3: Modulus of hopping tight binding impurity model (3d)

The modulus of hopping $W_{\mathbf{m}}$ is plotted as a function of $|\mathbf{m}|$ in figure 4.3. It shows that hopping is short ranged.

Average IPR for 3d mapped tight-binding lattice

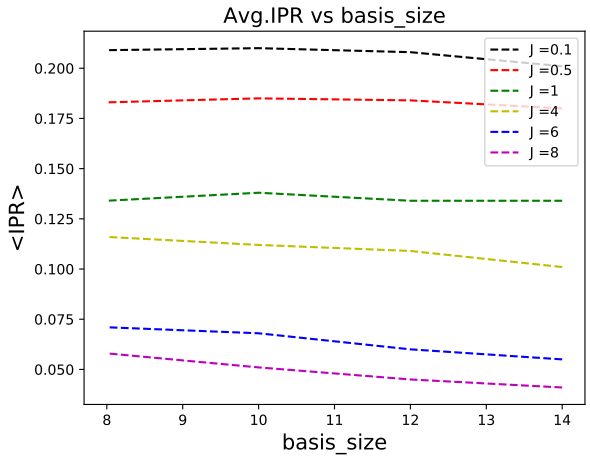

Figure 4.4: Average IPR vs system size (3d)

The average IPR is the IPR averaged over the eigenstates of Hamiltonian from equation (4.3.1). In the above figure 4.4 the average IPR is plotted versus linear size of the 3d tight binding model obtained.

From the figure 4.4 for lower values coupling strength (J) average IPR is almost a constant, as J is increased around $J = 4$ the average IPR exhibits a smooth scaling with the linear size of the system (L) and also average IPR $\to 0$ as size of the system is increased. This is signature of delocalisation in the system. There is not a clear distinction in average IPR to show a transition from localisation to delocalisation due to the limitation of linear size (L).

Average level spacing ratio for 3d mapped tight binding lattice

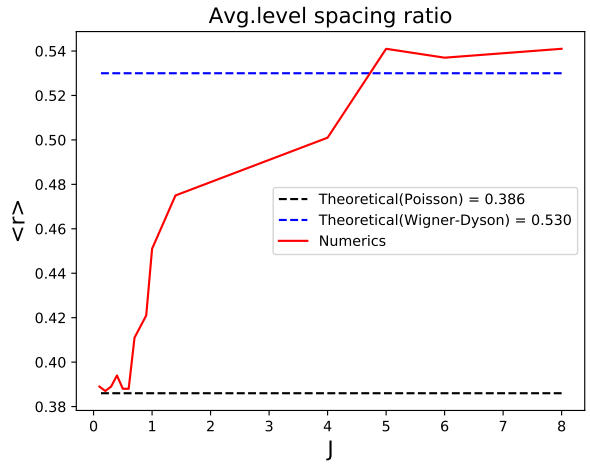

Figure 4.5: Average Level spacing ratio vs J (3d)

In the above figure 4.5 the variation of average IPR with coupling strength (J) is shown.

On increasing the coupling strength (J) there is a clear transition in average level spacing ratio from $< r > \approx 0.386$ (localised dynamics) to $< r > \approx 0.529$(diffusive dynamics) and this transition happens around $2 \leq J \leq 4$.

Average level spacing ratio of quantum kicked rotors

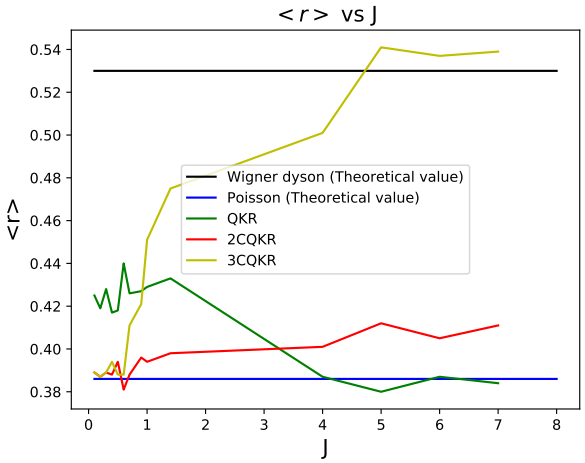

Figure 4.6: Average level spacing ratio vs J (1d,2d and 3d)

In the above figure 4.6 the average level spacing ratio versus coupling strength is plotted for the tight-binding lattice models in 1d,2d and 3d obtained from quantum kicked rotors with and without coupling. In the case of the tight-binding lattice (1d) obtained from single quantum kicked rotor without coupling, we have taken $J = K$. The abbreviations used in the figure 4.6 is as follows

QKR: Quantum kicked rotor without any coupling, 2CQKR: Two spatially coupled quantum kicked rotors and 3CQKR: Three spatially coupled quantum kicked rotors.

There is clear transition in the average level spacing ratio from $< r > \approx 0.386$ to $< r > \approx 0.530$ on increasing the coupling strength (J) only in the case of 3d tight-binding model, this dynamics is similar to the Anderson impurity model as there is a metal-insulator transition observed on increasing the disorder strength (W) in the case of 3d, not in 1d and 2d lattice. The main distinction in the transition in our tight-binding model is it's from insulator(dynamical localisation) to metal (dynamical delocalisation) on increasing the coupling strength rather than metal-insulator in the Anderson model.

5 Quantum Resonance

In this chapter different types of quantum resonance in the kicked rotor is explained.

$$H(t) = \frac{L^2}{2} + K\cos\theta \sum_n \delta(t-n)$$

Solving the Schrodinger equation with the above-kicked rotor Hamiltonian, a relation between the wave function after one kick ($\bar{\phi}(\theta)$) and the initial wavefunction ($\phi(\theta)$) can be obtained and given below in equations (5.0.1) and (5.0.2).

$$\bar{\phi}(\theta) = \exp(-i\tilde{K}\cos\theta) \sum_{n=-\infty}^{\infty} A_n \exp\left(-i\frac{\hbar n^2}{2} + in\theta\right) \tag{5.0.1}$$

where $\tilde{K} = \frac{K}{\hbar}$

$$A_n = \frac{1}{2\pi}\int_0^{2\pi} \phi(\theta) e^{-in\theta} d\theta \tag{5.0.2}$$

The wavefunction in equation (5.0.1) is invariant under the substitution $\hbar = \hbar + 4m\pi$, m is an integer. Therefore it's sufficient to consider the values of $\hbar$ on the interval (0,4π).

The relation between Fourier components separated by one kick is given by

$$\bar{A}_n = \sum_{m=-\infty}^{\infty} F_{\mathrm{nm}} A_m \tag{5.0.3}$$

The Floquet matrix elements is given by

$$F_{nm} = (-i)^{n-m} \exp\left(-i\frac{\hbar}{2}m^2\right) J_{n-m}(\tilde{K}) \tag{5.0.4}$$

where, $J_{n-m}(\tilde{K})$ is a First order Bessel function.

5.1 Primary Resonance ($\hbar = 4\pi m$)

The wave function after one kick from equation (5.0.1) is of the from

$$\bar{\phi}(\theta) = \exp(-i\tilde{K}\cos\theta)\phi(\theta) \tag{5.1.1}$$

Energy of the kicked rotor can be calculated by:

$$E(t) = -\frac{\hbar^2}{2}\int_0^{2\pi} \phi^*(\theta,t)\frac{\partial^2}{\partial\theta^2}\phi(\theta,t) \tag{5.1.2}$$

Long time average of energy goes as

$$E(t) = K^2t^2/4 \tag{5.1.3}$$

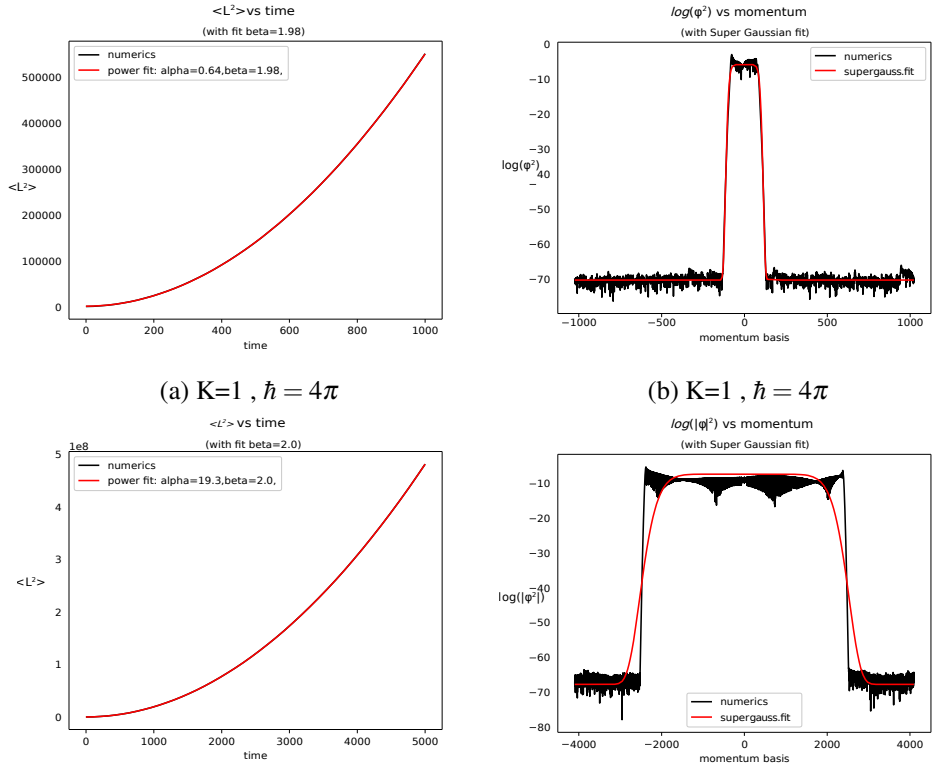

(a) K=1 , $\hbar = 4\pi$

(b) K=1 , $\hbar = 4\pi$

(c) K=6, $\hbar = 4\pi$

(d) K=6, $\hbar = 4\pi$

Figure 5.1: Primary quantum resonance

In the above figure 5.1 $< L^2 >$ is plotted versus time and the final momentum density in log scale ($\log(\phi_m^2(t))$) after 5000 kicks in case primary resonance is shown. In the figures 5.1 (a) and (c) , we can see that the energy goes as t^2 at long times with the hep of a power law fit($< L^2 > \approx \alpha t^\beta$), and figures (b) and (d) the $log(\phi_m^2(t))$ has a Super Gaussian fit implying the diffusive dynamics of the system.

Super Gaussian in momentum space:

$$f(m) = A\exp\left(-\left(\frac{(m-m_o)^2}{2\sigma^2}\right)^P\right)$$

where P = 4,6,8,.. m_0 is the center of super Gaussian, σ is the standard deviation and P is the degree of the super Gaussian. This captures the diffusive dynamics in momentum space of kicked rotor.

5.2 Secondary resonances ($\hbar = 4\pi\frac{p}{q}$)

where p, q are non zero integers and they are not equal.

The wave function after one kick $\bar{\phi}(\theta)$ is

$$\bar{\phi}(\theta) = \exp(-i\tilde{K}\cos\theta)\cdot F(\theta) \tag{5.2.1}$$

where

$$F(\theta) = \sum_{n=-\infty}^{\infty} A_n \exp\left(-i\frac{2\pi p}{q}n^2 + in\theta\right) \tag{5.2.2}$$

$$A_n = \frac{1}{2\pi}\int_0^{2\pi} \phi(\theta)e^{-in\theta}d\theta \tag{5.2.3}$$

In general the wave function evolution can be done by a scattering matrix S [23]

$$\bar{\phi}\left(\theta + \frac{2\pi m}{q}\right) = \sum_{n=0}^{q-1} S_{mn}\phi\left(\theta + \frac{2\pi n}{q}\right) \tag{5.2.4}$$

At large time energy goes as

$$E(t) = \eta t^2 + at + b + E(0) \tag{5.2.5}$$

Therefore the quasi-energy spectrum in resonance is continuous, besides the continuous component, the spectrum may have discrete levels [23]. (if $\hbar = 4\pi\frac{p}{q}$ it has no more than q-1 discrete levels)

$K \ll q$

$$\eta \sim \left(\frac{K}{q}\right)^{2q} \tag{5.2.6}$$

$K \gg q$

$$\eta \approx \frac{K^2}{\xi q} \tag{5.2.7}$$

where ξ is a constant independent of K and q.

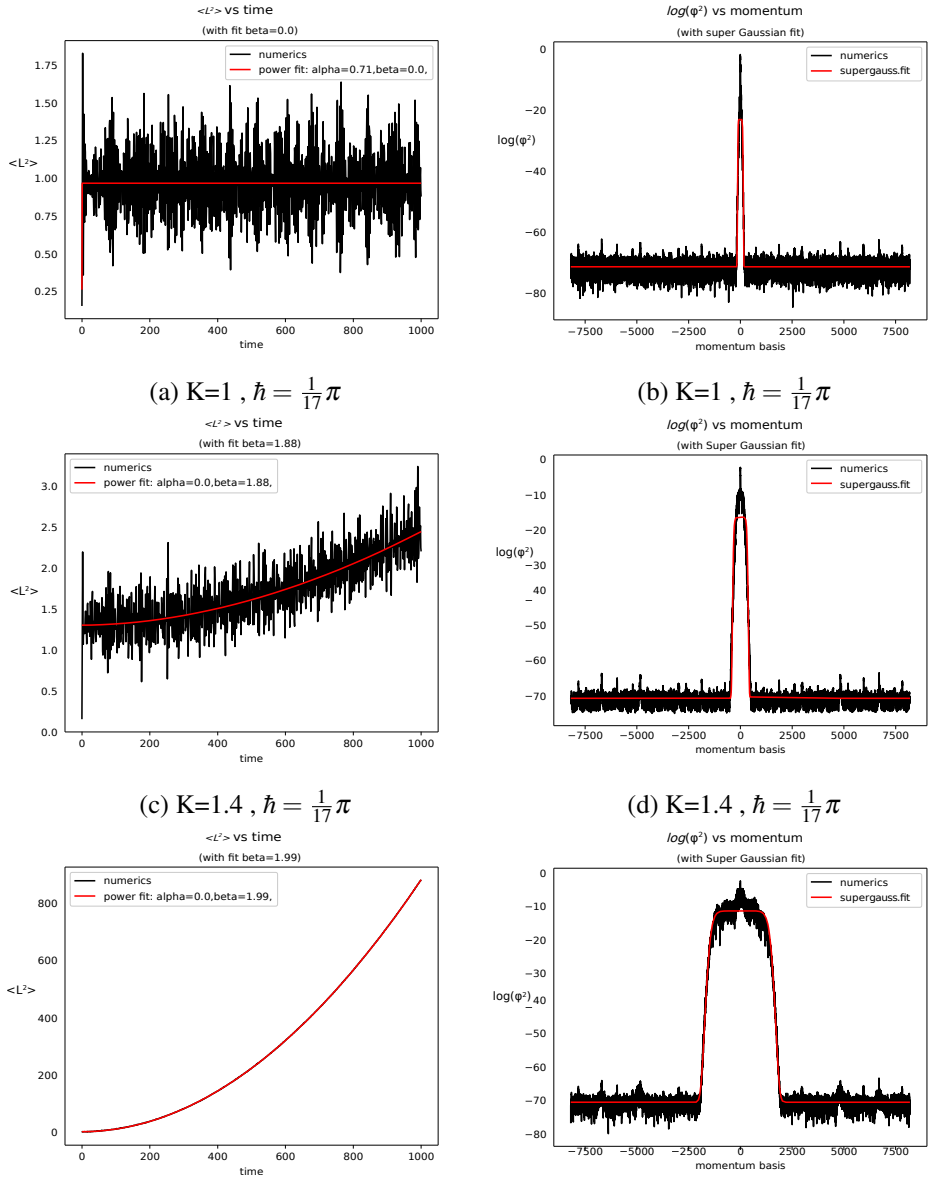

(a) K=1 , $\hbar = \frac{1}{17}\pi$

(b) K=1 , $\hbar = \frac{1}{17}\pi$

(c) K=1.4 , $\hbar = \frac{1}{17}\pi$

(d) K=1.4 , $\hbar = \frac{1}{17}\pi$

(e) K=2 , $\hbar = \frac{1}{17}\pi$

(f) K=2 , $\hbar = \frac{1}{17}\pi$

Figure 5.2: Secondary quantum resonance

In the above figure 5.2 the behaviour of $< L^2 >$ and $\log(|\phi(t)|^2)$ are shown for $\hbar$ commensurate with π ($\hbar = \frac{1}{17}\pi$), $\frac{K}{q} = \frac{1}{68}$ in (a) and (b), $\frac{K}{q} = \frac{1.4}{68}$ in (c) and (d), $\frac{K}{q} = \frac{2}{68}$ in (e) and (f) is plotted.

From the above plots it is clearly seen that the coefficient (η) of t^2 in long time average energy equation (5.2.5) follows the dependence explained in equation (5.2.6) [$\eta \sim (\frac{K}{q})^{2q}$].

5.3 Anti-resonance ($\hbar = 2\pi$)

From equation (5.0.1) the Wave function after one kick is given by:

$$\bar{\phi}(\theta) = \exp(-iK\cos\theta)\phi(\theta+\pi) \tag{5.3.1}$$

The quasi-energy spectrum has only two discrete levels.

The eigenfunctions are

$$\Phi_{\varepsilon_1}(\theta) = g_{\pm}(\theta)(1 \pm \exp(-iK\cos(\theta))) \tag{5.3.2}$$

$$\Phi_{\varepsilon_2}(\theta) = g_{\pm}(\theta)(1 \mp \exp(-iK\cos(\theta))) \tag{5.3.3}$$

where $g_{\pm}(\theta+\pi) = \pm g_{\pm}(\theta)$

Every level is infinitely degenerate and Φ_{ε_1} and Φ_{ε_2} for a complete set.

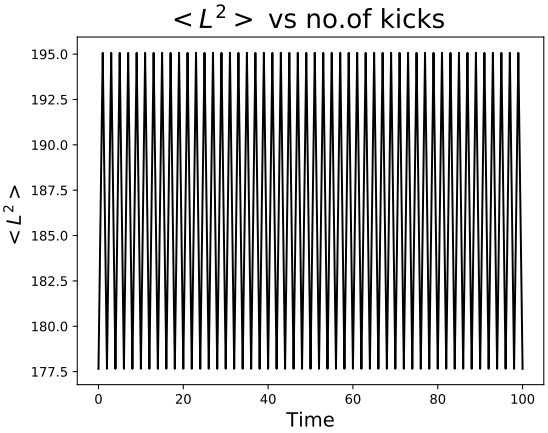

Figure 5.3: Anti-resonance

In the figure 5.3 $< L^2 >$ is plotted versus time for K = 6 and $\hbar = 2\pi$. The dynamics are localised when $\hbar = 4m\pi + 2\pi$, where m is any positive integer. The spectrum has only two discrete levels. Its seen that system returns to the initial state after alternate kicks.

6 Quantum resonances in spatially coupled kicked rotors

In this chapter quantum resonance in spatially coupled kicked rotors is studied and its distinction from quantum resonance in kicked rotor is shown.

6.1 Quantum resonance in Two spatially coupled kicked rotors

$$H = \frac{L_1^2}{2} + \frac{L_2^2}{2} + [K_1\cos(\theta_1) + K_2\cos(\theta_2) + J\cos(\theta_1+\theta_2)] \sum_{n=-\infty}^{\infty} \delta(t-n) \tag{6.1.1}$$

Let the initial wavefunction be $\phi(\theta_1,\theta_2)$, we evolve it with the floquet operator and $\bar{\phi}(\theta_1,\theta_2)$ be the wavefunction after one kick.

$$\begin{aligned}\bar{\phi}(\theta_1,\theta_2) = &\exp(-i\tilde{K_1}\cos\theta_1 - i\tilde{K_2}\cos\theta_2 - i\tilde{J_1}\cos(\theta_1+\theta_2)) \\ &\sum_{n_1,n_2=-\infty}^{\infty} A_{n_1,n_2}\exp\left(-\frac{i\hbar}{2}\left(n_1^2+n_2^2\right) + (n_1\theta_1 + n_2\theta_2)\right)\end{aligned} \tag{6.1.2}$$

where $\tilde{K_{1,2}} = K_{1,2}/\hbar$, $\tilde{J} = J/\hbar$

$$A_{n_1,n_2} = \left(\frac{1}{2\pi}\right)^2 \int_0^{2\pi}\int_0^{2\pi} \phi(\theta_1,\theta_2) e^{-i(n_1\theta_1+n_2\theta_2)} d\theta_1 d\theta_2 \tag{6.1.3}$$

A_{n_1,n_2} is the Fourier component of wavefunction $\phi(\theta_1,\theta_2)$, In our numerical calculation we have taken the range of momentum in two directions (n_1,n_2) same. This is reason why we observe primary quantum resonance for $\hbar = 2\pi$ rather than anti-resonance observed in normal quantum kicked rotor.

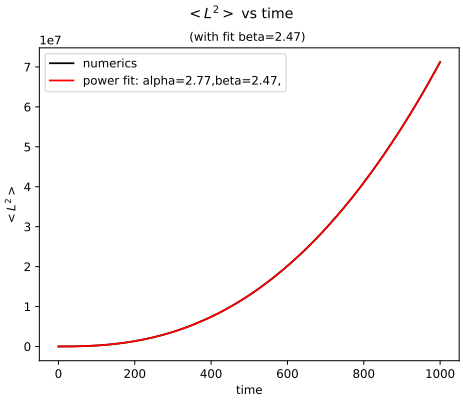

(a) $< L^2 >$ vs time, $\hbar = 2\pi$

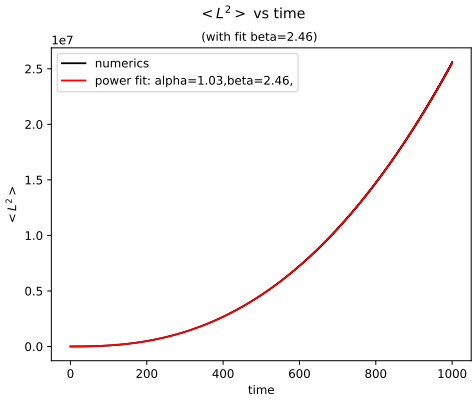

(b) $< L^2 >$ vs time, $\hbar = \pi$

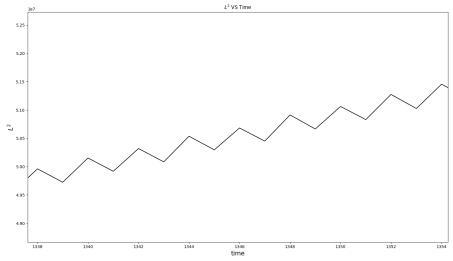

(c) A zoomed region from (b)

Figure 6.1: Quantum resonance in two spatially coupled kicked rotors

In the above figure 6.1 $< L^2 >$ is plotted versus time along one direction (a) for $\hbar = 2\pi$,(b) for $\hbar = \pi$. The power law fit in figure 6.1 (a) and (b) :$< L^2 > \approx \alpha t^{\beta}$

Quantum resonance is observed for both (a) $\hbar = 2\pi$ and (b) $\hbar = \pi$. But when $\hbar = \pi$ quantum resonance is observed with a flip in energy at each kick (c) this behaviour can be attributed to the interplay between the periodic terms with two different periods in the kicking potential, this behaviour is also observed at values $\hbar = \pi + 4m\pi$, where m is any positive integer. This behaviour is not seen when $\hbar = 2\pi$ as both the periodic functions in kicking potential is periodic with 2π.

Energy of the kicked rotor along a direction i $(i = 1,2)$ can be calculated by:

$$E_i(t) = -\frac{\hbar^2}{2}\int_0^{2\pi} \phi^*(\theta_1,\theta_2,t)\frac{\partial^2}{\partial\theta_i^2}\phi(\theta_1,\theta_2,t)d\theta_1 d\theta_2 \tag{6.1.4}$$

Long time average of energy numerically calculated goes as for $\hbar = 2\pi$ and $\hbar = \pi$:

$$E_i(t) \approx C_i t^{2.5} \tag{6.1.5}$$

where C_i is a constant determined by the kicking and coupling strengths of the system. The dependence of C_i on K and J is not very clear as the integral in equation (6.1.4) is not trivial.

6.2 Quantum resonance in Three spatially coupled kicked rotors

$$H = \frac{L_1^2}{2} + \frac{L_2^2}{2} + \frac{L_3^2}{2} + [K_1\cos(\theta_1) + K_2\cos(\theta_2) + K_3\cos(\theta_3) + J[\cos(\theta_1+\theta_2) + \cos(\theta_2+\theta_3) + \cos(\theta_1+\theta_3))] \sum_{n=-\infty}^{\infty} \delta(t-n) \tag{6.2.1}$$

Let the initial wavefunction be $\phi(\theta_1,\theta_2,\theta_3)$, we evolve it with the floquet operator. $\bar{\phi}(\theta_1,\theta_2,\theta_3)$ be the wavefunction after one kick.

$$\bar{\phi}(\theta_1,\theta_2,\theta_3) = \exp(-i\tilde{K_1}\cos\theta_1 - i\tilde{K_2}\cos\theta_2 - i\tilde{K_3}\cos\theta_3 - i\tilde{J_1}[\cos(\theta_1+\theta_2) + \cos(\theta_2+\theta_3) + \cos(\theta_1+\theta_3)] \sum_{n_1,n_2,n_3=-\infty}^{\infty} A_{n_1,n_2,n_3} \exp\left(-\frac{i\hbar}{2}\left(n_1^2+n_2^2+n_3^2\right) + (n_1\theta_1 + n_2\theta_2 + n_3\theta_3)\right)$$

where $\tilde{K_1} = \frac{K_1}{\hbar}$, $\tilde{K_2} = \frac{K_2}{\hbar}$, $\tilde{K_3} = \frac{K_3}{\hbar}$, $\tilde{J} = \frac{J}{\hbar}$

$$A_{n_1,n_2,n_3} = \left(\frac{1}{2\pi}\right)^3 \int_0^{2\pi}\int_0^{2\pi}\int_0^{2\pi} \phi(\theta_1,\theta_2,\theta_3) e^{-i(n_1\theta_1+n_2\theta_2+n_3\theta_3)} d\theta_1 d\theta_2 d\theta_3 \tag{6.2.2}$$

A_{n_1,n_2,n_3} is the Fourier component of wavefunction $\phi(\theta_1,\theta_2,\theta_3)$, In our numerical calculation we have taken the same range of momentum in three directions (n_1,n_2,n_3). So we will observe primary quantum resonance at $\hbar = \frac{4\pi}{3}$.

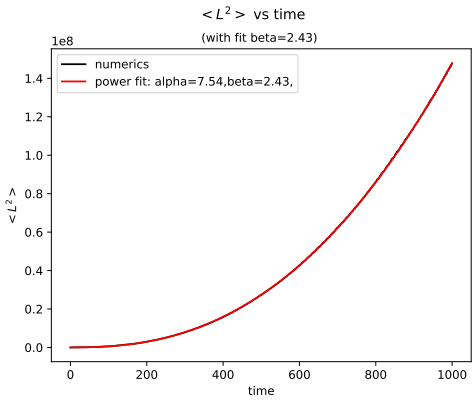

(a) $< L^2 >$ vs time $\hbar = \frac{4\pi}{3}$

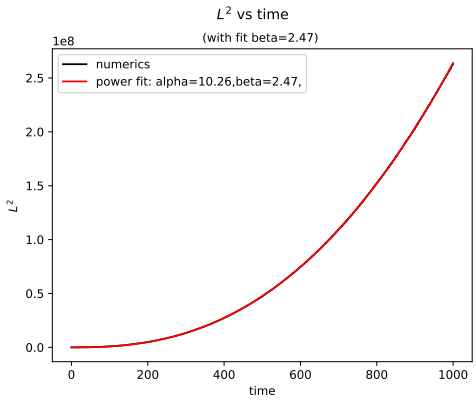

(b) $< L^2 >$ vs time, $\hbar = \frac{2\pi}{3}$

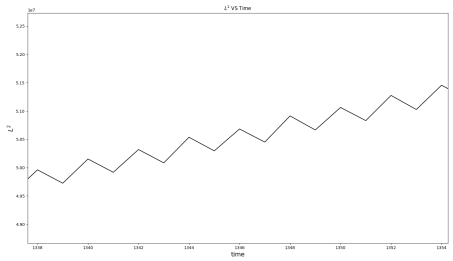

(c) A zoomed region from (b)

Figure 6.2: Quantum resonance in three spatially coupled kicked rotors

In the above figure 6.2 $< L^2 >$ is plotted versus time along one direction for with a power law fit for $\hbar = \frac{4\pi}{3}$ (a), $\hbar = \frac{2\pi}{3}$ (b) and (c) is a zoomed plot (b) for $\hbar = \frac{2}{3}\pi$. Power law fit in figure 6.2: $< L^2 >= \alpha t^{\beta}$

At $\hbar = \frac{2}{3}\pi$ we observe quantum resonance, but there is also a flip in energy seen at every kick. This behaviour is also observed at values $\hbar = (\frac{2}{3})\pi + 4m\pi$, where m is any positive integer. But this flipping in energy is not observed in the primary resonance case $(\hbar = \frac{4\pi}{3})$.

Long time average of energy numerically calculated goes as for $\hbar = \frac{4\pi}{3}$ and $\hbar = \frac{2\pi}{3}$:

$$E_i(t) \approx C_i t^{2.5} \tag{6.2.3}$$

where E_i is the average energy along any one directions, C_i is a constant depending on kick strength (K) and coupling strength (J).

Summary on resonance in coupled kicked rotors

In the below table we have mentioned the minimum values of $\hbar$ required to observed the following phenomenon.

QKR: quantum kicked rotor without coupling, 2CQKR: Two spatially coupled quantum kicked rotor, 3CQKR: Three spatially coupled quantum kicked rotor.

Anti-resonance in spatially coupled kicked rotor means resonance with a phase flip at every kick.

Quantum resonance	QKR	2CQKR	3CQKR
Primary resonance	4π	2π	$\frac{4\pi}{3}$
Anti-resonance	2π	π	$\frac{2\pi}{3}$

7 Quasi-periodic or Temporally coupled kicked rotor

In this chapter quasi-periodic or temporally coupled kicked rotor system is studied. By adding temporal modulation in the kick strength quasi-periodic kicked rotor can be obtained from the standard kicked rotor. We have dealt with two and three incommensurate frequencies systems using split technique and exact diagonalisation of mapped tight-binding models.

Hamiltonian of Quasi-periodic kicked rotor with three incommensurate frequencies (2π,ω_2,ω_3)

$$H_{\text{qp}} = \frac{L^2}{2} + \bar{K}(t)\cos\theta \sum_n \delta(t-n) \tag{7.0.1}$$

where

$$\bar{K}(t) = K\left[1 + \varepsilon\cos(\omega_2 t + \varphi_2)\cos(\omega_3 t + \varphi_3)\right] \tag{7.0.2}$$

The classical evolution equations are given by:

$$\begin{cases} L_{n+1} = L_n + \bar{K}(t)\sin\theta_n \\ \theta_{n+1} = \theta_n + L_{n+1} \end{cases} \tag{7.0.3}$$

The only problem here in equation (7.0.3) is that the kick strength is time-dependent. Now we use the mapping of this quasi-periodic kicked rotor onto a 3d kicked pseudo-rotor with the special initial condition of a plane wave[24]. Pseudo-rotor is another form of spatially coupled kicked rotor hence we can approach the quasi-periodic kicked rotor model similar to spatially coupled kicked rotor in the above chapters.

$$H = \frac{L_1^2}{2} + \omega_2 L_2 + \omega_3 L_3 + K\cos\theta_1\left[1 + \varepsilon\cos\theta_2\cos\theta_3\right]\sum_n \delta(t-n) \tag{7.0.4}$$

This is called a pseudo rotor because of the presence of unusual kinetic energy terms linear in momentum. But this is a periodic time with constant kicking strengths K and ε, so we can easily write the iteration map.

The advantage of the quasi-periodic kicked rotor is that the dynamics can be numerically generated very easily, because it requires only one spatial dimension, but displays the richness of 3d systems.

7.1 Classical Quasi-periodic Kicked rotor

Equations of motion obtained from canonical equations of 3d-pseudo kicked rotor:

$$L_{n+1}^{(1)} = L_n^{(1)} + K \sin\theta_n^{(1)} \left(1 + \varepsilon \cos\theta_n^{(2)} \cos\theta_n^{(3)}\right)$$

$$L_{n+1}^{(2)} = L_n^{(2)} + K\varepsilon \cos\theta_n^{(1)} \sin\theta_n^{(2)} \cos\theta_n^{(3)}$$

$$L_{n+1}^{(3)} = L_n^{(3)} + K\varepsilon \cos\theta_n^{(1)} \cos\theta_n^{(2)} \sin\theta_n^{(3)}$$

$$\theta_{n+1}^{(1)} = \theta_n^{(1)} + L_{n+1}^{(1)}$$

$$\theta_{n+1}^{(2)} = \theta_n^{(2)} + \omega_2$$

$$\theta_{n+1}^{(3)} = \theta_n^{(3)} + \omega_3$$

The last two equations are trivially integrated $\theta_n^{(2)} = \theta_0^{(2)} + n\omega_2$ and similarly for θ_3 . If we now start with the initial condition $\theta_0^{(2)} = \phi_2$, $\theta_0^{(3)} = \phi_3$, this mapping is the same as the original quasi-periodic kicked rotor.

The classical dynamics of the kicked pseudo-rotor along any direction is identical to the one of the quasi-periodically kicked rotor.

Plots of Classical Quasi-periodic kicked rotor

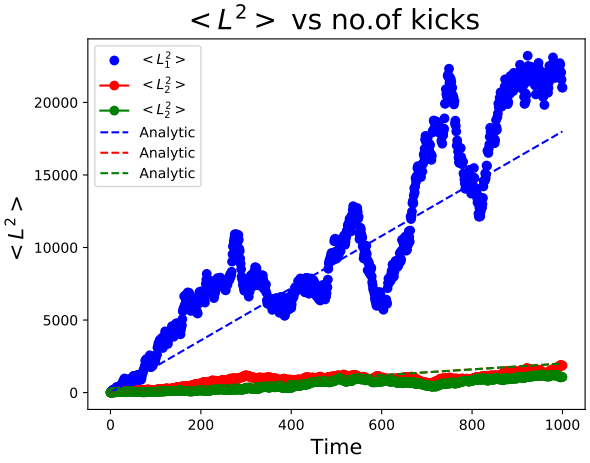

Figure 7.1: $< L^2 >$ vs time for Classical Quasi-periodic kicked rotor

In the above figure 7.1 $< L^2 >$ measure of average energy versus time is plotted along three directions for K = 8, ε = 0.5 along with a analytic fit using the diffusion constant calculated below.

The diffusion constants calculated up to first order approximation are given by:

$$D_1 = \frac{K^2}{2}(1+\frac{\varepsilon^2}{4})$$

$$D_2 = \frac{K^2\varepsilon^2}{8}$$

$$D_3 = \frac{K^2\varepsilon^2}{8}$$

7.2 Quantum Quasi periodic kicked rotor with two incommensurate frequencies (2QPKR)

$$H_{\text{qp}} = \frac{L^2}{2} + \bar{K}(t)\cos\theta \sum_n \delta(t-n) \tag{7.2.1}$$

where

$$\bar{K(t)} = K[1+\varepsilon\cos(\omega_2 t+\varphi_2)] \tag{7.2.2}$$

We have obtained the below plots using split techniques, similar to the ones used in kicked rotor case. Similar to the case of spatially coupled kicked rotor initial wavefunction is a Gaussian centred around zero momentum.

Here $\omega_2 = \sqrt{2}$

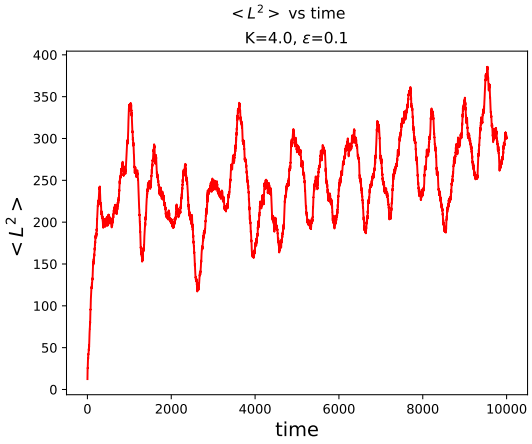

(a) K=4, ε = 0.1

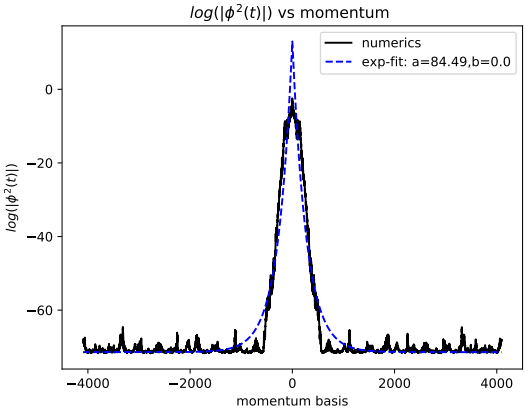

(b) K=4, ε = 0.1, Time = 10000

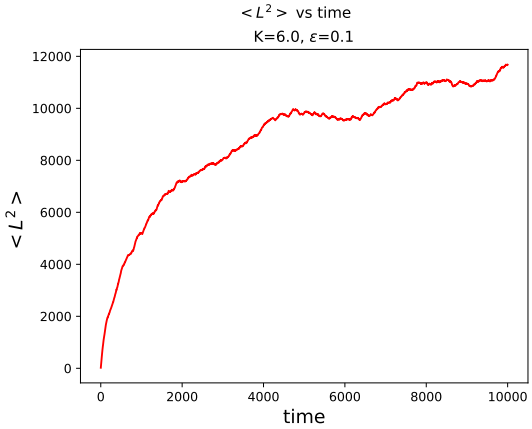

(c) K=6, $\varepsilon = 0.1$

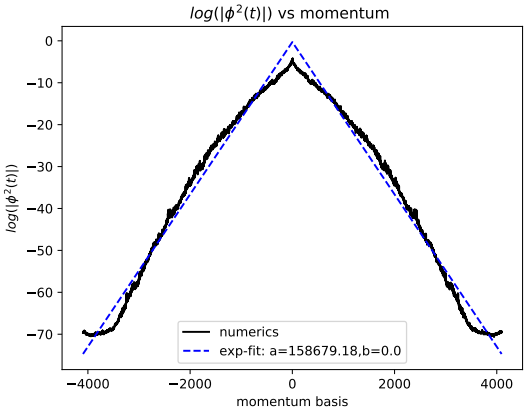

(d) K=6, $\varepsilon = 0.1$, Time = 10000

Figure 7.2: Dynamics of quasi-periodic kicked rotor with 2 incommensurate frequencies

The above figure 7.2 the $< L^2 >$ vs time and final momentum density after 10000 kicks $|\phi_m^2(t)|$ in log scale is plotted for a fixed $\varepsilon = 0.1$ and two different kicking strengths K = 4 and 6.

As K increases the width of the exponential density profile increases, but it doesn't become completely diffusive as the average energy is still localised in the long time limit.

7.3 Quantum Quasi-periodic kicked rotor with three incommensurate frequencies(3QPKR)

In this case the kicking is of the form

$$\bar{K(t)} = K[1 + \varepsilon \cos(\omega_2 t + \varphi_2)\cos(\omega_3 t + \varphi_3)] \tag{7.3.1}$$

where,
$\omega_2 = \sqrt{2}$
$\omega_3 = \sqrt{3}$

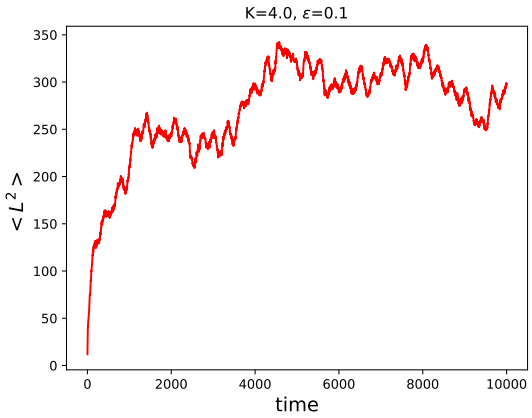

(a) K=4, $\varepsilon = 0.1$

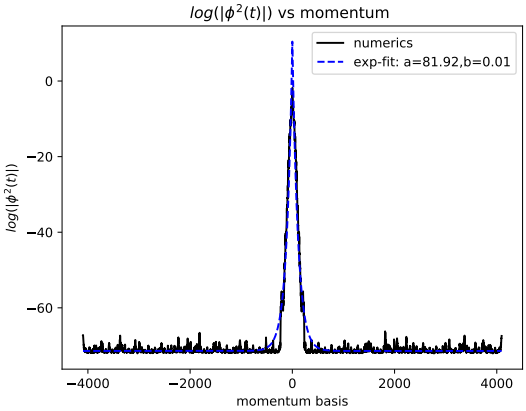

(b) K=4, $\varepsilon = 0.1$

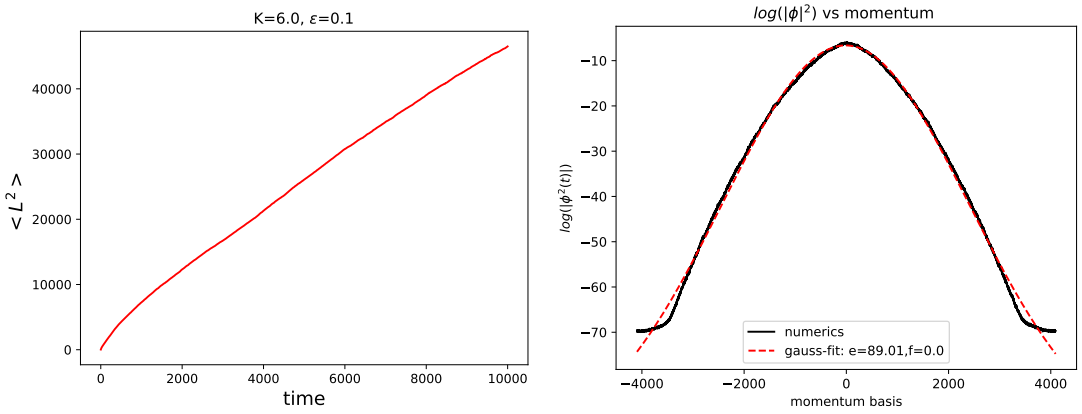

(c) K=6, $\varepsilon = 0.1$ (d) K=6, $\varepsilon = 0.1$

Figure 7.3: Dynamics of quasi-periodic kicked rotor with 3 incommensurate frequencies

In the above figure 7.3 $< L^2 >$ versus time and final momentum density $(|\log(\phi^2(t))|)$ after 10000 kicks is plotted for a fixed coupling strength ($\varepsilon = 0.1$)

For kick strength $(K = 4)$ the dynamics is localised in momentum space as seen from (a) and (b). When the kick strength is increased to $K = 6$ the dynamics become completely diffusive at long time limit and the momentum density is Gaussian as shown in (c) and (d).

7.4 Mapping quasi-periodic to tight binding impurity model

The quantum dynamics of the periodically kicked pseudo-rotor can be obtained by Floquet states via mapping to a 3d Anderson-like model.

$$H = \frac{L_1^2}{2} + \omega_2 L_2 + \omega_3 L_3 + K\cos\theta_1\left[1 + \varepsilon\cos\theta_2\cos\theta_3\right]\sum_n \delta(t-n) \tag{7.4.1}$$

The analogy between the quasi-periodic kicked rotor and a 3d kicked rotor with an initial condition taken as "plane wave source". Let's consider an initial state

$$\Phi(\theta_1,\theta_2,\theta_3,t=0) \equiv \phi(\theta_1,t=0)\,\delta(\theta_2-\varphi_2)\,\delta(\theta_3-\varphi_3) \tag{7.4.2}$$

The above-mentioned state is completely localized in θ_2 and θ_3 and completely delocalized in the conjugate momenta L_2 and L_3. A simple calculation shows that the stroboscopic evolution of Φ under the pseudo-kicked rotor in equation (7.4.1) is the same as evolving the initial state $\phi(\theta_1,t=0)$ under the original quasi-periodic Hamiltonian [11][24].

From a stroboscopic point of view, the time evolution of Φ is determined by the floquet operator.

$$F = e^{-i\frac{K}{\hbar}\cos\theta_1(1+\varepsilon\cos\theta_2\cos\theta_3)} \times e^{-i\hbar\left(L_1^2/2+\omega_2 L_2+\omega_3 L_3\right)} \tag{7.4.3}$$

$$\Phi(\theta_1,\theta_2,\theta_3,t) = F^t\Phi(\theta_1,\theta_2,\theta_3,t=0) \tag{7.4.4}$$

Using this floquet operator and the initial wavefunction, a mapping between the 3d pseudo-kicked rotor and 3d Anderson type model can be obtained. The steps in this calculation are exactly similar to the mapping between the kicked rotor and 1d Anderson type model [9].

$$T_{\mathbf{m}}\Phi_{\mathbf{m}} + \sum_{\mathbf{r}\neq 0} W_{\mathbf{r}}\Phi_{\mathbf{m}-\mathbf{r}} = -W_{\mathbf{0}}\Phi_{\mathbf{m}} \tag{7.4.5}$$

where $\mathbf{m} \equiv (m_1, m_2, m_3)$ and $\mathbf{r}$ label sites in a 3d lattice in momentum space.

The on-site energy T_{m} is given by

$$T_{\mathrm{m}} = \tan\left\{\frac{1}{2}\left[\omega - \left(\frac{\hbar m_1^2}{2} + \omega_2 m_2 + \omega_3 m_3\right)\right]\right\} \tag{7.4.6}$$

$$W(\theta_1,\theta_2,\theta_3) = \tan\left[K\cos\theta_1\left(1+\varepsilon\cos\theta_2\cos\theta_3\right)/2\hbar\right] \tag{7.4.7}$$

The hopping matrix elements in momentum space $W_{\mathbf{r}}$

$$W_{\mathbf{r}} = \int_0^{2\pi} \frac{d\theta_1 d\theta_2 d\theta_3}{2\pi} e^{-\imath(r_1\theta_1+r_2\theta_2+r_3\theta_3)} W(\theta_1,\theta_2,\theta_3) \tag{7.4.8}$$

It should be noted that the 3d aspect comes from the presence of three frequencies in the dynamical system: the usual "momentum frequency"– present in the standard kicked rotor equation and two additional time frequencies ω_2 and ω_3. Thus, increasing the number of incommensurate frequencies allow one to tune the effective dimensionality of the system.

In our calculation we have taken $(\hbar, \omega_2, \omega_3, \pi)$ are incommensurate with each other[1]. When the above conditions are true, then there exists a metal-insulator transition as predicted for the 3d Anderson model are expected.

[1] If any of $(\hbar, \omega_2, \omega_3, \pi)$ is commensurate with other the dynamics enter quantum resonance regime and there no metal-insulator transition in this case

7.5 Level spacing ratio for Mapped 3d tight-binding Hamiltonian

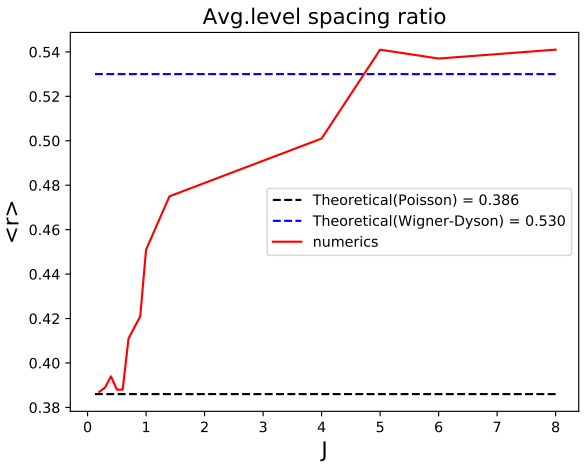

Figure 7.4: Average Level spacing ratio of tight binding impurity model obtained from 3d Pseudo-kicked rotor

The quantum dynamics of a quasi-periodic kicked rotor with 3 incommensurate frequencies can be studied using the 3d pseudo kicked rotor, which in turn can be mapped to a 3d tight binding model in momentum space as explained in section (7.4).

In figure 7.4 the average level spacing ratio is plotted as a function of coupling strength (J), there is a transition from Poisson($< r >= 0.386$) to Wigner Dyson($< r >= 0.530$) in level spacing around $J = 5$ as a indication of localisation-delocalisation transition in quasi-periodic kicked rotor with 3 incommensurate frequencies.

8 Coupled kicked rotors in momentum space

In this section we have studied two and three kicked rotors coupled in momentum space and the mapping to an interacting Aubry-Andre model is also studied. The main aim is to check the existence of Many-body dynamical localisation in two and three coupled kicked rotors.

The Hamiltonian of N coupled kicked rotor in momentum space:

$$H(t) = \tilde{K}(\hat{\mathbf{L}}) + V(\hat{\theta})\sum_{n}\delta(t-nT) \tag{8.0.1}$$

where $\hat{\mathbf{L}} = (\hat{L_1}, \hat{L_2}, ...\hat{L_N})$ and $\hat{\theta} = (\hat{\theta_1}, \hat{\theta_2}, ...\hat{\theta_N})$

The kinetic energy part $(\tilde{K}(\hat{\mathbf{L}}))$ consist of two parts the non-interacting part $(\tilde{K_0}(\hat{\mathbf{L}}))$ and interacting part $(\tilde{K'}(\hat{\mathbf{L}}))$ arising due to nearest neighbour interaction in momentum space.

8.1 Mapping kicked rotors coupled in momentum space to interacting tight binding model

A analytic mapping of coupled N quantum kicked rotors in momentum space and interacting variant of Aubry-Andre model with N particles which can support MBL[12].

The floquet operator corresponding to the above mentioned Hamiltonian (8.0.1)

$$F = e^{-\imath\frac{V(\hat{\theta})}{\hbar}} e^{-\imath\frac{\tilde{K}(\hat{\mathbf{L}})T}{\hbar}} \tag{8.1.1}$$

$$\hat{F}|A\rangle = \mathrm{e}^{-\mathrm{i}\phi}|A\rangle \tag{8.1.2}$$

where $|A\rangle$ is a Floquet state and ϕ is their corresponding eigenphase.

In interaction picture, the above floquet equation becomes

$$\mathrm{e}^{\mp\mathrm{i}\hat{K}T/(2\hbar)}\mathrm{e}^{\mp\frac{\mathrm{i}}{\hbar}V(\hat{\theta})}\mathrm{e}^{\mp\mathrm{i}\hat{K}T/(2\hbar)}|\tilde{A}\rangle = \mathrm{e}^{\mp\mathrm{i}\phi}|\tilde{A}\rangle \tag{8.1.3}$$

where $|\tilde{A}\rangle = \mathrm{e}^{\mathrm{i}\hat{K}T/(2\hbar)}|A\rangle$

Let us define the local angular momentum eigenstates for N quantum kicked rotors. $|\tilde{\mathbf{m}}\rangle = |\tilde{m}_1, \tilde{m}_2, \ldots, \tilde{m}_N\rangle$

When the non-interacting kinetic energy part acts on the angular momentum state, $\tilde{K}_0 = \frac{1}{2}\sum_{i=1}^{N} \hat{L}_i^2$ and $\tilde{K}_0|\tilde{\mathbf{m}}\rangle = 2\hbar\varphi(\tilde{\mathbf{m}})|\tilde{\mathbf{m}}\rangle$, where $\varphi(\tilde{\mathbf{m}}) \equiv \frac{\hbar}{4}\sum_{i=1}^{N} \tilde{m}_i^2$.

similarly when the interacting part of kinetic energy acts on local momentum states, $\tilde{K}'|\tilde{\mathbf{m}}\rangle = 2\hbar\varphi'(\tilde{\mathbf{m}})|\tilde{\mathbf{m}}\rangle$

The explicit form of kinetic energy due to coupling in momentum space $\hat{K}'$ is not defined, but assumed that K' commutes with unperturbed kinetic energy($\tilde{K}_0$), i.e.. $\left[\hat{K}_0, \hat{K}'\right] = 0$.

Let's define $\Phi(\tilde{\mathbf{m}}) \equiv \varphi(\tilde{\mathbf{m}}) + \varphi'(\tilde{\mathbf{m}})$, from the equation (8.1.3) inserting completeness condition in local momentum states and projecting $\langle\tilde{n}|$ from left, we obtain the following equation:

$$\begin{array}{c}\left(-\mathrm{e}^{\pm \mathrm{i}\phi} + \left\langle \tilde{\mathbf{n}} \middle| \hat{F}_{\pm} \middle| \tilde{\mathbf{n}} \right\rangle\right) \langle \tilde{\mathbf{n}}|\tilde{A}\rangle \\ + \sum_{\tilde{\mathbf{m}}\neq\tilde{\mathbf{n}}} \mathrm{e}^{\mathrm{i}[\Phi(\mathbf{n})-\Phi(\mathbf{m})]} \left\langle \tilde{\mathbf{n}} \middle| \hat{F}_{\pm} \middle| \tilde{\mathbf{m}} \right\rangle \langle \tilde{\mathbf{m}}|\tilde{A}\rangle = 0\end{array} \tag{8.1.4}$$

where $\hat{F}_{+} = \hat{F}^{\dagger}, \quad F_{-} = \hat{F}$.

Following relations are straight forward $\langle\tilde{\mathbf{n}}|\hat{F}|\tilde{\mathbf{m}}\rangle = \mathrm{e}^{-2\mathrm{i}\Phi(\tilde{\mathbf{n}})} \left\langle \tilde{\mathbf{n}} \middle| \mathrm{e}^{-\frac{i}{\hbar}V(\hat{\theta})} \middle| \tilde{\mathbf{m}} \right\rangle$ and $\left\langle \tilde{\mathbf{n}} \middle| \hat{F}^{\dagger} \middle| \tilde{\mathbf{m}} \right\rangle = \mathrm{e}^{2\mathrm{i}\Phi(\tilde{\mathbf{m}})} \left\langle \tilde{\mathbf{n}} \middle| \mathrm{e}^{\frac{i}{\hbar}V(\hat{\theta})} \middle| \tilde{\mathbf{m}} \right\rangle$.

The above equation (8.1.4) can be rewritten in the following way:

$$h_{\tilde{\mathbf{n}}} c_{\tilde{\mathbf{n}}} + \sum_{\tilde{\mathbf{m}}\neq\tilde{\mathbf{n}}} W_{\tilde{\mathbf{n}},\tilde{\mathbf{m}}} c_{\tilde{\mathbf{m}}} = \cos(\phi) c_{\tilde{\mathbf{n}}} \tag{8.1.5}$$

Where $c_{\tilde{n}} = \left\langle \tilde{n} \middle| \tilde{A} \right\rangle$ and $h_{\tilde{n}}$ represents the on-site potential and $W_{\tilde{\mathbf{n}},\tilde{\mathbf{m}}}$ represents the hopping potential given by.

$$W_{\mathbf{n},\tilde{\mathbf{m}}} = \mathrm{Re}\left\{ \mathrm{e}^{\mathrm{i}[\Phi(\tilde{\mathbf{n}})+\Phi(\tilde{\mathbf{m}})]} \int_0^{2\pi} \frac{\mathrm{d}^N\theta}{(2\pi)^N} \mathrm{e}^{\frac{i}{\hbar}V(\theta)} \mathrm{e}^{-\mathrm{i}(\tilde{\mathbf{n}}-\tilde{\mathbf{m}})\cdot\theta} \right\} \tag{8.1.6}$$

The above equation (8.1.5) looks like a N-body Schrodinger equation with onsite potential $h_{\tilde{m}}$ and eigenvalues $\cos\phi$

In order to make lattice with interactions lets label $h_{\tilde{n}} \equiv \varepsilon(\tilde{n}) + V(\tilde{n})$

From equation(8.1.6)

$$\int_0^{2\pi} \frac{d^N\theta}{(2\pi)^N} \cos\left[\frac{V(\theta)}{\hbar} + 2\varphi(\tilde{\mathbf{n}}) + 2\varphi'(\tilde{\mathbf{n}})\right] \quad = \varepsilon(\tilde{\mathbf{n}}) + V(\tilde{\mathbf{n}}) \tag{8.1.7}$$

The above equation (8.1.7) determines the type of lattice models we can map to as the left-hand side of the above equation is bounded by the range of quasi-energies[1].

The interaction operator can be tuned to get the desired lattice, for example when $V(\tilde{\mathbf{n}}) = 0$, we can set $\varphi'(\tilde{\mathbf{n}}) = 0$ in which case reduces to

$$\varepsilon(\tilde{\mathbf{n}}) = \int_0^{2\pi} \frac{\mathrm{d}^N\theta}{(2\pi)^N} \cos\left[\frac{V(\theta)}{\hbar} + 2\varphi(\tilde{\mathbf{n}})\right] \tag{8.1.8}$$

[1] Defined up to only modulo $2\pi\hbar/T$

From equations (8.1.7) and (8.1.8) we can obtain a exact solution to determine $\varphi'(n)$.

$$\cos\left[2\varphi'(\tilde{\mathbf{n}})\right] + \Gamma_1(\tilde{\mathbf{n}})\sin\left[2\varphi'(\tilde{\mathbf{n}})\right] = \Gamma_2(\tilde{\mathbf{n}}) \tag{8.1.9}$$

where

$$\Gamma_1 = -\frac{\int_0^{2\pi}\frac{d^N\theta}{(2\pi)^N}\sin\left[\frac{V(\theta)}{\hbar}+2\varphi(\tilde{\mathbf{n}})\right]}{\int_0^{2\pi}\frac{d^N\theta}{(2\pi)^N}\cos\left[\frac{V(\theta)}{\hbar}+2\varphi(\tilde{\mathbf{n}})\right]}$$

$$\Gamma_2 = 1 + \frac{V(\tilde{\mathbf{n}})}{\int_0^{2\pi}\frac{d^N\theta}{(2\pi)^N}\cos\left[\frac{V(\theta)}{\hbar}+2\varphi(\tilde{\mathbf{n}})\right]}$$

$$2\varphi'(\tilde{\mathbf{n}}) = \arctan\left[\frac{\pm\Gamma_1\gamma+\Gamma_2}{\Gamma_1\Gamma_2\mp\gamma}\right] \in [-\pi,\pi] \tag{8.1.10}$$

where $\gamma \equiv \sqrt{1+\Gamma_1^2-\Gamma_2^2}$.

For the N kicked rotors without any spatial coupling $V(\theta) = \hbar\sum_{l=1}^{N} k^{(l)}\cos(\theta_l)$.

This implies

$$\Gamma_1 = \tan[2\varphi(\tilde{\mathbf{n}})], \tag{8.1.11}$$

$$\Gamma_2 = 1 + V(\tilde{\mathbf{n}})/\left\{\cos[2\varphi(\tilde{\mathbf{n}})]\prod_{l=1}^{N} J_0\left(\left|k^{(l)}\right|\right)\right\}. \tag{8.1.12}$$

Where $J_0(k)$ is Bessel function of first kind of zeroth order.

In thermodynamic limit as $N \to \infty$ the product $\prod_{l=1}^{N} J_0\left(\left|k^{(l)}\right|\right)$ vanishes, which enforces $V(\tilde{n}) \to 0$.

Hence it's not possible to map the contact interactions in lattice to kicked rotor coupled in momentum space in the thermodynamic limit.

8.2 Two kicked rotors coupled in momentum space (2MQKR)

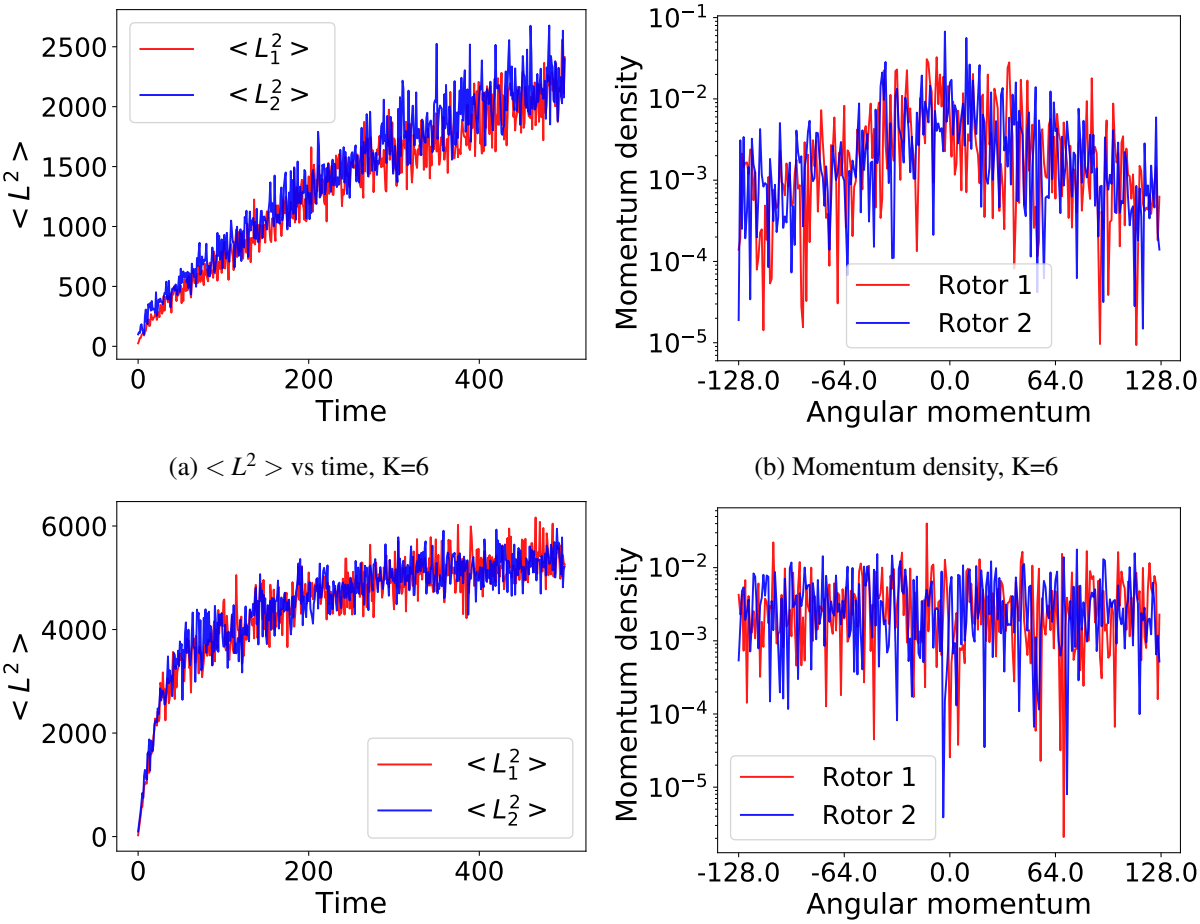

(a) $< L^2 >$ vs time, K=6

(b) Momentum density, K=6

(c) $< L^2 >$ vs time, K= 16

(d) Momentum density, K=16

Figure 8.1: Dynamics of Two kicked rotors coupled in momentum space $V(\tilde{\mathbf{n}}) = 0.005$

In the above figure 8.1 $< L^2 >$ vs time and the final momentum density $|\phi^2_{\tilde{\mathbf{n}}}(t)|$ is plotted after 400 kicks for a fixed interaction strength $V(\tilde{\mathbf{n}}) = 0.005$.

It's seen for lower values of kicking (K=6) (b) the momentum density has an exponential profile indicating the presence of MBDL phase. When kicking strength is increased (K=16) (d) the momentum density becomes uniform, indicating the destruction of the MBDL phase. Role of Truncation error can be significant.

8.3 Three kicked rotors coupled in momentum space (3MQKR)

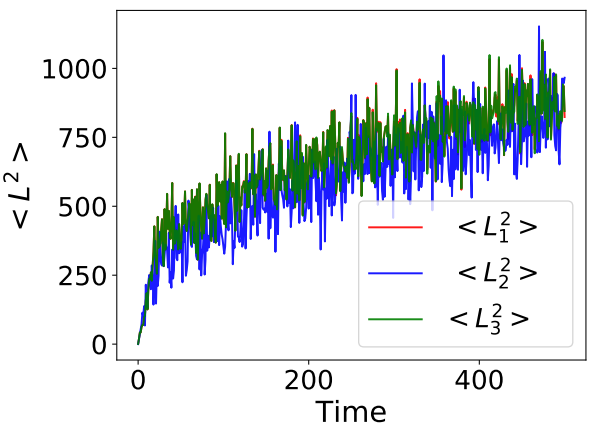

(a) $< L^2 >$ vs time, K=6

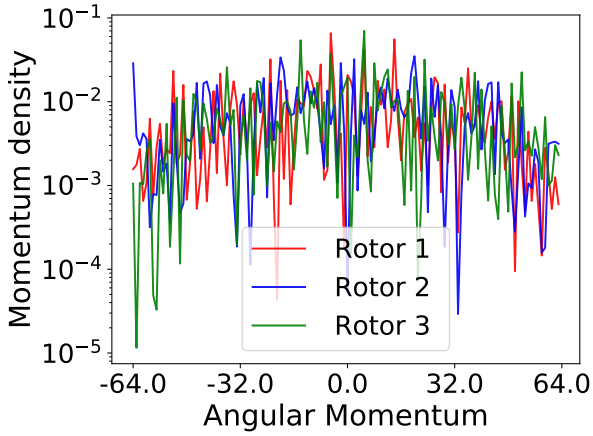

(b) Momentum density, K=6

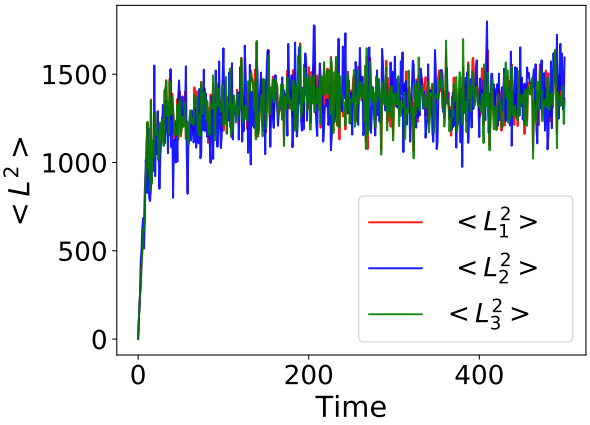

(c) $< L^2 >$ vs time, K=16

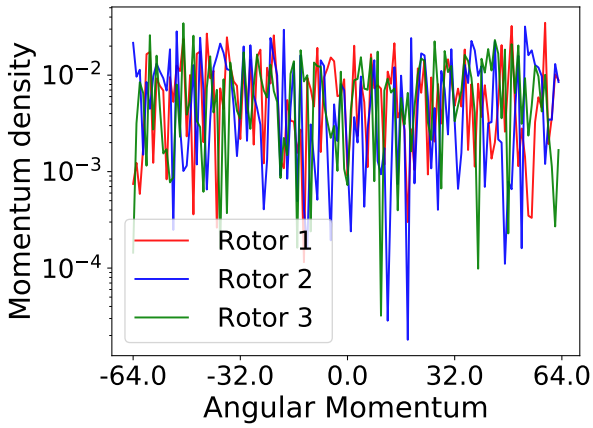

(d) Momentum density, K=16

Figure 8.2: Dynamics of Three kicked rotors coupled in momentum space $V(\mathbf{n}) = 0.\ 005$

In the above figure 8.2 $< L^2 >$ vs time and final momentum density $|\phi^2_{\tilde{\mathbf{n}}}(t)|$ is plotted after 400 kicks for a fixed interaction strength $V(\tilde{\mathbf{n}}) = 0.005$. Figure 8.2 depicting the dynamics of Three kicked rotors coupled in momentum space shows a similar behaviour as the Two kicked rotors coupled in momentum space in figure 8.1. There is the destruction of the MBDL phase on increasing the kicking strength in the presence of weak interaction($V(\mathbf{n}) = 0.005$). We need to increase the basis size to avoid the Truncation error but its computationally expensive.

9 Conclusions

This thesis is devoted to studying kicked rotors with coupling. We have started with a thorough analysis of the kicked rotor model in quantum and classical regime. Although most of the work done there are well established it helped us to understand more intricate details to the calculations we used and it acted as a testing background for our numerical techniques.

The first type of coupling we considered between the rotors is spatial and of the form $\cos(\theta_i + \theta_j)$, this form is chosen to make the coupling nonlinear and keep the model non-integrable. We studied mainly two and three coupled rotors using this form of coupling. We have obtained the behaviour of average energy and time evolved momentum density using split techniques and its observed in case of three coupled kicked rotors for large coupling strengths there is an unbound energy growth for a long time (time much longer than the break time) but this is not observed in case of two coupled kicked rotors. This phenomenon can be explained by extending the map between a kicked rotor and a tight binding impurity model[9] to coupled kicked rotors. We have obtained the map between two and three coupled kicked rotors to 2d and 3d time-independent tight binding impurity model (similar to the Anderson impurity model). The main things to be check in the mapped lattice model are the presence of random or quasi-random onsite potentials and short-ranged hopping. The form of interactions decides the type of lattice in the time-independent impurity model. By studying the spectral statistics of the mapped lattice model we see a clear indication for the transition between dynamically localized to delocalized phase in case of three coupled kicked rotor model. This map can be extended between N-spatially coupled kicked rotors and N-dimensional impurity model, there is localisation-delocalisation transition for $N \geq 3$ coupled kicked rotors. As $N \to \infty$ the dynamics is expected to become delocalized in momentum space[10]. We also observe a behaviour similar to weak localisation in 2d Anderson model for large kick strengths in two coupled kicked rotor dynamics. So in contrast with the behaviour of a quantum kicked rotor which always shows localised behaviour in momentum space, we obtain new phenomenology arising when the interactions are added a kicked rotor mainly localized and delocalized phases are observed.

Quantum resonance in kicked rotor occurs when the effective plank constant of the system is commensurate with 4π, except for odd integer multiples of 2π where anti-resonance [23] is observed. We have extended the study of quantum resonance in two and three spatially coupled kicked rotors, and there is phase flip at every kick but the average behaviour is super-ballistic for effective plank constant of the system ($\alpha = \hbar = \frac{2\pi}{N}$), where N is the number of spatially coupled kicked rotors.

The quasi-periodic kicked rotor or temporally coupled kicked rotor with two and three incommensurate frequencies has been studied. As the quasi-periodic kicked rotor has a continuous-time dependence other than delta kick time dependence, it becomes a little hard to obtain dynamics using the general techniques used for the kicked rotor. So to study quasi-periodic we establish a mapping to a pseudo-rotor model which have only delta-kick time dependence's under special initial conditions. This pseudo-rotor with two and three incommensurate frequencies is used to study the behaviour of corresponding quasi-periodic kicked rotor in the classical and quantum regime. We have also studied the map between

the pseudo-kicked rotor and a tight binding impurity model similar to the one obtained for spatially coupled kicked rotors. A localisation-delocalisation transition is observed in the quasi-periodic kicked rotor with three incommensurate frequencies on increasing the kick strength but not in case of the quasi-periodic kicked rotor with two frequencies. This is not surprising now as the number of incommensurate frequencies in quasi-periodic kick rotor corresponds to the number of kicked rotors coupled spatially in pseudo kicked rotor, which in turn corresponds to the dimensionality of the mapped impurity lattice model.

At last, we studied the model of kicked rotors coupled in momentum space[12], which has a map to interacting Aubry-Andre model. This map is not valid in the thermodynamic limit i.e... $N \to \infty$ where N is the number of kicked rotors coupled. We have primarily studied two and three momentum coupled kicked rotors, the exact form of momentum coupling is not described but the eigenphases obtained by acting the interaction term in kinetic energy operator (arise only due to momentum coupling) can be obtained analytically for weak interaction strength in corresponding mapped lattice model. For weak interaction strength in the mapped lattice model, a localisation-delocalisation transition is observed two and three momenta coupled kicked rotors for large values of kick strengths.

The punch line of this thesis is due to the absence of conservation of energy in periodically kicked systems with added interactions, they are expected to heat up indefinitely but this is not the case always. As there exists a regime in parameter space of the system where dynamical localisation is present even with interactions present in the system and this has been verified in systems with spatial, temporal and momentum interactions.

Future directions

The weak localisation limit which is present in two spatially coupled kicked rotor is not very well studied. Scaling theory analysis in this regime might help us to understand more about the role of coupling in the absence of dynamical localisation. Multi-fractal analysis can be done in the regime of transition from dynamical localisation-delocalisation in coupled kicked rotor.

Spectral statistics of momentum coupled kicked rotors can be done. To characterise MBL phases in kicked rotors coupled in momentum space quasi-local integrals of motion can be constructed. New models with kicking potentials different from the standard kicked rotor can be used to make the mapped lattice interacting even in the thermodynamical limit.

The quantum resonance in spatially coupled kicked rotors can be experimentally realised using cold atoms setup.

Bibliography

[1] Hans-Jürgen Stöckmann. *Quantum chaos*. First Edition, 1999.

[2] D'Alessio L. Bukov, M. and Polkovnikov. Universal high-frequency behavior of periodically driven systems: from dynamical stabilization to floquet engineering. *Advances in Physics*, 64,139-226, (2015).

[3] Kitagawa T. Alicea J. Akhmerov A. R. Pekker D. Refael G. Cirac J. I. Demler E. Lukin M. D. Jiang, L. and P. Zoller. Majorana fermions in equilibrium and in driven cold-atom quantum wires. *Phys. Rev. Lett.*, 106 , 220402, (2011).

[4] Claassen M. Sentef M. A. Kennes, D. M. and C. Karrasch. Light- induced d-wave superconductivity through floquet-engineered fermi surfaces in cuprates. *ArXiv e-prints*, (2018).

[5] Weiss. C Eckardt. A and Holthaus. M. Superfluid-insulator transition in a periodically driven optical lattice. *Phys. Rev. Lett*, 95,260404, (2005).

[6] Chan C.-K. Alpichshev Z. Gardner D. Lee Y. Lee P. A. Mahmood, F. and N. Gedik. elective scattering between floquet-bloch and volkov states in a topological insulator. *S. Nature Physics*, 12:306, (2016).

[7] L. D'Alessio and M. Rigol. Long-time behavior of isolated periodically driven interacting lattice systems. *Phys. Rev. X*, 4,041048, (2014).

[8] Papic Z.-Huveneers F. Ponte, P. and D. A Abanin. Many-body localization in periodically driven systems. *OPhys. Rev. Lett.*, 114,140401, (2015).

[9] D.R. Grempel S. Fishman and R.E. Prange. Chaos, quantum recurrences and anderson localization. *Phys. Rev. Lett*, 49:509, (1982).

[10] Davide Rossini Rosario Fazio Alessandro Silva Simone Notarnicola, Fernando Iemini and Angelo Russomanno. From localization to anomalous diffusion in the dynamics of coupled kicked rotors. *Phys.Rev.E*, 97,0222002, (2018).

[11] J.Wang and A.M.Garcia-Garcia. The anderson transition in a 3d kicked rotor. *Phys.Rec.E 79,036206*, (2009).

[12] L.A.Toikka and A.Andreanov. Many body dynamical localisation of coupled quantum kicked rotors. *arXiv:1901.09362v1*, (2019).

[13] Grebogi C. Wisdom J. Shinbrot, T. and J. A. Yorke. Chaos in a double pendulum. *American Journal of Physics*, 60,491-499, (1992).

[14] M. V.. Berry. Regularity and chaos in classical mechanics, illustrated by three deformations of a circular 'billiard'. *American Journal of Physics*, 2,91, (1981).

[15] M. V Berry. Semiclassical mechanics of regular and irregular motion. (1983).

[16] A. Politi. Lyapunov exponent. *Scholarpedia*, 8(3):2722, 2013. revision #137286.

[17] C. F. Bharucha Bala Sundaram F. L. Moore, * J. C. Robinson and M. G. Raizen. Atom optics realization of the quantum δ-kicked rotor. *Phys.Rev.Lett*, 75, 25, (1995).

[18] L. Moorman P.M. Koch EJ. Galvez, B.E. Sauer and D. Richards. Microwave ionization of h atoms: Breakdown of classical dynamics for high frequencies. *Phys. Rev.lett*, 61,2011, (1988).

[19] C. Bharucha P.E. Williams F.L. Moore, J.C. Robinson and M.G. Raizen. Observation of dynamical localization in atomic momentum transfer: A new testing ground for quantum chaos. *Phys. Rev.lett*, 73,2974, (1994).

[20] Linda E.Reichl. The transition to chaos, conservative classical systems and quantum manifestations. *Second Edition*, (2004).

[21] P. W. Anderson. Absence of diffusion in certain random lattices. *Phys. Rev*, 109(5), 1492-1505, (1958).

[22] O. Giraud Y. Y. Atas, E. Bogomolny and G. Roux. Distribution of the ratio of consecutive level spacings in random matrix ensembles. *Phys. Rev. Lett. 110,084101*, (2013).

[23] Shepelyanskii D.L Izrailev, F.M. Quantum resonance for a rotator in a nonlinear periodic field. *Theor Math Phys*, 43, 553–561, (1980).

[24] Guarneri.I Casati.G and Shepelyansky.D. L. Anderson transition in a one-dimensional system with three in-commensurable frequencies. *Phys. Rev. Lett.62345–8*, (1989).